9 Microphysical Processes in Cold Clouds

As discussed in Chapter 8, warm cloud microphysics and rain formation is not sufficient to explain most global precipitation, in particular over the continents (Mülmenstädt et al., 2015). In fact, 50 % of global precipitation events of more than 1 mm day^{-1} involve cold clouds (Field and Heymsfield, 2015; Heymsfield et al., 2020), denoting clouds containing ice. In the tropics, precipitation via the ice phase accounts for 69 % of the total precipitation amount (Lau and Wu, 2003) and in midlatitudes for more than 90 % of the total precipitation (Löhnert et al., 2015), with the rest from warm rain. In midlatitudes, warm rain is rare, especially over land. This phenomenon is consistent with the droplet size distributions of continental cumuli being shifted toward smaller sizes as compared to clouds over oceans (Figure 1.22). In continental clouds, ice phase processes need to take over for precipitation formation. Low ice crystal number concentrations on the order of 1 L^{-1} can already initiate ice microphysical processes and precipitation (Rangno and Hobbs, 1988). The cloud phase not only matters for precipitation formation, but is also important for, for example, cloud electrification, and determines the optical properties of the clouds, which influences the radiative budget in the current climate (Chapter 2) and in a future, warmer climate (Chapter 12).

Once a cloud extends to altitudes where the temperature is below 0 °C, ice crystals may form by homogeneous or heterogeneous ice nucleation, as will be discussed in Section 9.1. Heterogeneous ice nucleation takes place with the help of INPs and can occur via different pathways depending on the temperature and ice supersaturation (Section 9.1.2). By contrast, homogeneous ice nucleation usually occurs without an INP at temperatures below −38 °C.

Once nucleated, the ice particles can grow by diffusion from the vapor phase (Figure 9.1b), leading to crystals with different habits (Sections 9.2 and 9.3). In stratiform clouds, ice crystals mainly grow by aggregation to form snowflakes (Figure 9.1e and Chapter 10). In convective clouds, ice crystals mainly grow by riming, leading to the formation of graupel or hail, (Chapters 10 and 11), but mixed habits, such as rimed snowflakes also exist. Riming denotes the collision of a liquid hydrometeor (cloud droplet, drizzle drop, raindrop) with a solid hydrometeor (ice crystal, snowflake, graupel, hail), with subsequent freezing of the liquid hydrometeor (Figure 9.1f). The counterpart of raindrop break-up in warm clouds (Figure 9.1g) is ice multiplication in cold clouds (Figure 9.1h–j, Section 9.4), which can occur upon collision and drastically increase the number concentration of ice crystals in the cloud. The melting and/or sublimation of ice and snow (Section 9.5) completes our discussion of microphysical processes including the ice phase. A summary of all microphysical processes is given in Section 9.6.

https://doi.org/10.1017/9781009485654.010 Published online by Cambridge University Press

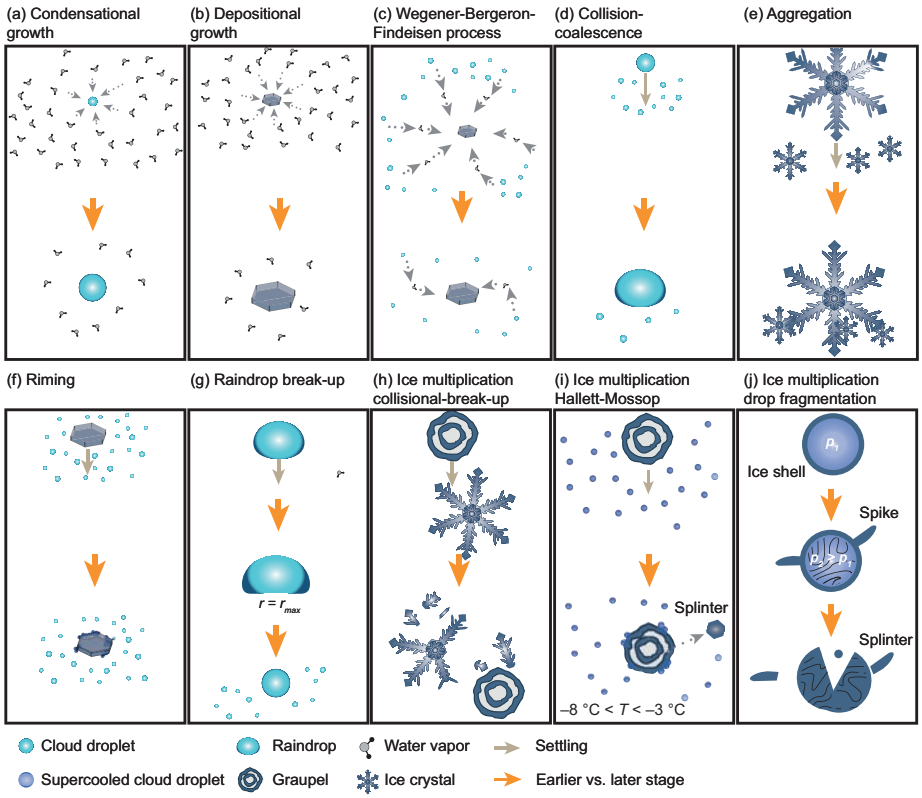


Figure 9.1 Schematic of the different microphysical processes in an earlier and later stage: (a) condensational growth, (b) depositional growth, (c) Wegener–Bergeron–Findeisen process, (d) collision–coalescence, (e) aggregation, (f) riming, (g) raindrop break-up, and (h) ice multiplication due to collisional-break-up, (i) ice multiplication due to the Hallett–Mossop process, (j) ice multiplication due to droplet fragmentation upon freezing.

9.1 Ice Nucleation (Primary Ice Production)

Ice crystals can form in different ways in the atmosphere, broadly categorized as heterogeneous and homogeneous ice nucleation. *Heterogeneous ice nucleation* describes the formation of an ice phase, within a vapor or liquid phase, catalyzed by a foreign surface, a substance that can act as an INP (Vali et al., 2015). *Homogeneous ice nucleation*, by contrast, occurs when ice forms without a foreign surface, either through direct deposition of water vapor onto an ice embryo, or through the homogeneous freezing of cloud droplets or aqueous solution droplets.

In our atmosphere, the only homogeneous nucleation process of hydrometeors is homogeneous nucleation of ice crystals from the liquid phase (*homogeneous freezing*). In fact, neither cloud droplets nor ice crystals can form by homogeneous nucleation from the vapor phase, because the atmospheric RH does not get high enough. The homogeneous freezing of aqueous solution droplets is a prominent freezing process in cirrus clouds (Kärcher and Lohmann, 2002). Heterogeneous nucleation, can occur either from the vapor phase or the liquid phase

https://doi.org/10.1017/9781009485654.010 Published online by Cambridge University Press

in our atmosphere. Heterogeneous ice nucleation is the dominant ice nucleation process in mixed-phase clouds (Korolev et al., 2017), but also occurs in cirrus clouds (Cziczo et al., 2013).

An established theory to describe ice nucleation is *classical nucleation theory* (CNT), as detailed in, for example, Pruppacher and Klett (1997). In the following, we use CNT to derive expressions for homogeneous and heterogeneous ice nucleation. CNT assumes that ice crystals are spherical, although we will see in Section 9.2 that ice crystals exhibit various habits.

9.1.1 Homogeneous Ice Nucleation

Homogeneous Nucleation of Ice from the Vapor Phase

Despite it not taking place in the atmosphere, we nevertheless start by discussing homogeneous ice nucleation from the vapor phase, termed deposition nucleation, because it is conceptually similar to the homogeneous droplet nucleation discussed in Section 7.1. In fact, it can be described analogously to homogeneous cloud droplet nucleation by replacing the vapor–liquid phase transition with the vapor–ice phase transition and the parameters related to liquid water with those related to ice. Thus, for homogeneous deposition nucleation also a Kelvin effect exists, which is analogous to the Kelvin effect for cloud droplets (eq. 7.15) if approximating the small ice crystals as ice spheres. Thus, the equilibrium water vapor pressure over the surface of a small ice sphere is enhanced compared to that over a bulk ice phase, as shown in Figure 9.2.

At atmospheric pressure and at temperatures below 0 °C, the chemical potential and therefore the Gibbs free energy (Section 7.1) of the bulk ice phase are lower than those of the vapor phase. However, the formation of a new interface between the two phases increases the Gibbs free energy of the system. The change in Gibbs free energy to homogeneously nucleate ice directly from the vapor phase is:

$$\Delta G_{i,v} = \underbrace{-\frac{4\pi r^3 R_v T}{3\alpha_i} \ln S_i}_{\text{volume term}} + \underbrace{4\pi r^2 \sigma_{i,v}}_{\text{surface term}}, \tag{9.1}$$

where $\Delta G_{i,v}$ is the Gibbs free energy for the phase transition from vapor to ice and $\alpha_i = 1/\rho_i$ is the specific volume of ice, which has a slight temperature dependence (Appendix A.3). Moreover, $\sigma_{i,v}$ is the surface tension between ice and water vapor. For reference, some values of $\sigma_{i,v}$ are listed in Table 9.1, and a temperature-dependent parameterization is given in Appendix A.3. From now on, we assume that $\sigma_{i,v} \approx \sigma_{i,a}$, the surface tension between ice and air. Analogously to the liquid phase (eq. 7.15), we can take the derivative of eq. (9.1) with respect to r and equal it to zero, in order to obtain the Kelvin equation for the ice phase within air:

$$e_{s,i}(r) = e_{s,i}(\infty) \exp\left(\frac{2\sigma_{i,a}}{\rho_i R_v T r}\right). \tag{9.2}$$

https://doi.org/10.1017/9781009485654.010 Published online by Cambridge University Press

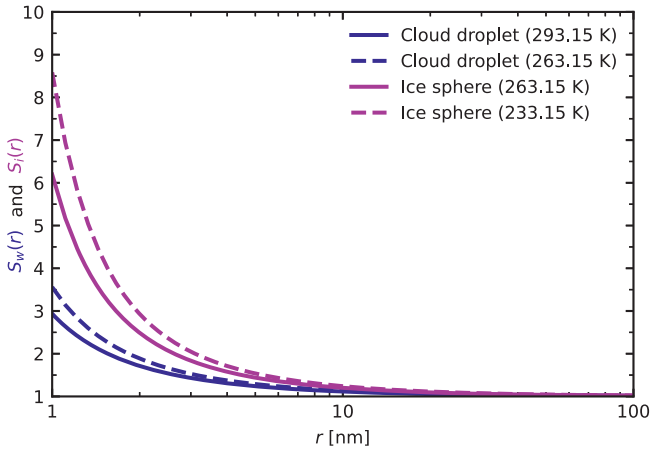


Figure 9.2 Kelvin's law giving the equilibrium saturation ratio as a function of radius for a cloud droplet at 293.15 K and 263.15 K and for an ice sphere at 263.15 K and 233.15 K, as calculated with eq. (7.15) and eq. (9.2), respectively. The vertical axis represents the equilibrium saturation ratio with respect to water $S_w(r)$ for a water droplet and with respect to ice $S_i(r)$ for an ice sphere. The temperature dependence of the ice density is taken from Pruppacher and Klett (1997) (eq. A.5) and that of the water density from Marcolli (2017) (eq. A.1). The values of the surface tension follow the parameterization of Vargaftik et al. (1983) (eq. A.12) for the interface of supercooled water and water vapor, and the parameterization given in Hale and Plummer (1974) (eq. A.13) for the interface of ice and water vapor.

At 273.15 K, $\sigma_{i,a}$ is approximately 100.03 mN m^{-1}. The surface tension between ice and air depends on temperature. Values of $\sigma_{i,a}$ can be estimated from combining CNT with measurements of homogeneous freezing of pure water droplets or $\sigma_{i,a}$ can directly be measured, but the estimates remain uncertain (McDonald, 1953; Ketcham and Hobbs, 1969). However, because ice has a larger volume than liquid water for the same mass at all $T < 0\,°C$ ($\alpha_i > \alpha_l$) and the surface tension between ice and air ($\sigma_{i,a}$) is larger than that between liquid water and air ($\sigma_{w,a}$), the Gibbs free energy barrier for the homogeneous nucleation of ice from the vapor phase is larger than that for homogeneous cloud droplet nucleation for the same saturation ratio S_i. Therefore, homogeneous nucleation of ice from the vapor phase is even less likely than homogeneous nucleation of liquid droplets in the atmosphere (Section 7.2, Table 7.1). For example, in order for a water droplet with $r = 2$ nm to be stable at 263.15 K, a saturation ratio with respect to water of $S_w = 1.8$ is needed. For a spherical ice crystal of the same radius, a saturation ratio with respect to ice of $S_i = 2.5$ (equivalent to $S_w = 2.24$) is required (Figure 9.2). This comparison is, however, not entirely accurate because in the atmosphere much higher supersaturations with respect to ice are found than supersaturations with respect to liquid water, owing to the scarcity of INPs. As S_i increases, the magnitude of the Gibbs free energy barrier decreases (eq. 9.1). Hence, the (homogeneous) nucleation of a new

https://doi.org/10.1017/9781009485654.010 Published online by Cambridge University Press

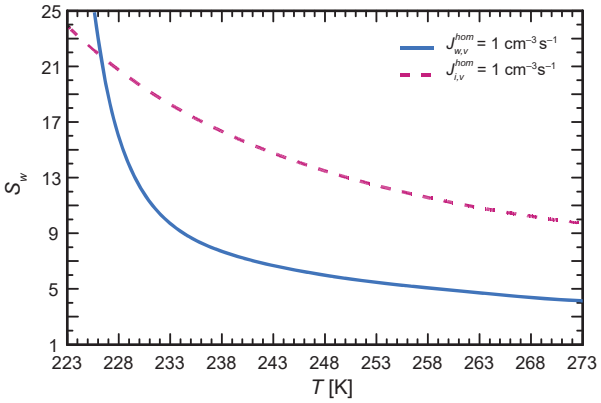


Figure 9.3 Saturation ratio with respect to liquid water S_w as a function of the temperature required to obtain a homogeneous nucleation rate of 1 cm^{-3} s^{-1} for liquid water from water vapor $J_{w,v}^{hom}$ and for ice from water vapor $J_{i,v}^{hom}$.

phase becomes statistically more likely. To compare the statistical likelihood of homogeneous droplet and ice crystal nucleation from the vapor phase, it is better to compare the saturation ratios necessary to generate a typical homogeneous nucleation rate J^{hom}. J^{hom} describes the number of nucleation events per unit volume and unit time in the parent phase. A nucleation rate on the order of $J^{hom} = 1\,\mathrm{cm}^{-3}\,\mathrm{s}^{-1}$ is required for nucleation from the vapor phase to occur on an atmospherically relevant time scale. The nucleation rate J^{hom} is given as:

$$J^{hom} = K_{kin} N_w \exp\left(-\frac{\Delta G^*}{k_B T}\right), \tag{9.3}$$

where ΔG^* is the Gibbs free energy barrier (critical Gibbs free energy) for the phase transition to occur, k_B is the Boltzmann constant, K_{kin} is the kinetic prefactor describing the diffusion rate at which water molecules are transferred into the ice embryo, and N_w is the number density of water molecules in the parent phase (Ickes et al., 2015).

The height of the Gibbs free energy barrier depends on substance-related quantities, such as the surface tension between the two phases, and on the conditions in the parent phase, such as temperature and supersaturation. These quantities are combined in the thermodynamic factor $\exp(-\Delta G^*/k_B T)$. For the homogeneous nucleation of ice from the vapor phase, the Gibbs free energy barrier $\Delta G_{i,v}^*$ can be determined from the maximum of eq. (9.1), analogous to the Gibbs free energy barrier for nucleation of cloud droplets from the vapor phase $\Delta G_{w,v}^*$ that can be determined from the maximum of eq. (7.13), and is given by (Ickes et al., 2015):

$$\Delta G_{i,v}^* = \frac{16\pi}{3} \frac{\alpha_i^2 \sigma_{i,a}^3}{(R_v T \ln S_i)^2}. \tag{9.4}$$

Figure 9.3 shows S_w, which is required to obtain a homogeneous nucleation rate for water in vapor of $J_{w,v}^{hom} = 1\,\mathrm{cm}^{-3}\,\mathrm{s}^{-1}$ and for ice in vapor of $J_{i,v}^{hom} = 1\,\mathrm{cm}^{-3}\,\mathrm{s}^{-1}$. Both nucleation rates require the same S_w at $T = 226\,\mathrm{K}$. At higher temperatures, the homogeneous nucleation of water is more favorable and at lower temperatures, the homogeneous nucleation of ice from the vapor phase is more favorable. However, the saturation ratios needed for both processes are much higher than those observed in Earth's atmosphere, causing both to be negligible.

https://doi.org/10.1017/9781009485654.010 Published online by Cambridge University Press

Homogeneous Nucleation of Ice from the Liquid Phase (Freezing)

In contrast to homogeneous ice nucleation from the vapor phase, homogeneous ice nucleation within a liquid phase, termed *homogeneous freezing*, is indeed observed in the atmosphere. When supercooling water, it changes its properties (Angell, 1982). As water is increasingly supercooled, the mobility of water molecules decreases, eventually allowing molecules to arrange into ice-like (ordered) structures, called ice embryos. If the ice embryo exceeds the critical radius at a given temperature and saturation ratio, it is called an *ice germ* or *critical ice embryo*, and homogeneous freezing of the whole droplet is initiated. Molecular dynamic simulations suggest that the nucleation of ice in supercooled water occurs in low-mobility regions (Fitzner et al., 2019). The Gibbs free energy for homogeneous freezing of a pure water droplet $\Delta G_{i,w}$ is given as:

$$\Delta G_{i,w} = -\frac{4\pi r^3 R_v T}{3\alpha_i} \ln \frac{e_{s,w}}{e_{s,i}} + 4\pi r^2 \sigma_{i,w}, \tag{9.5}$$

where $\sigma_{i,w}$ is the interfacial tension between ice and liquid water. The corresponding Gibbs free energy barrier $\Delta G^*_{i,w}$ is given by

$$\Delta G^*_{i,w} = \frac{16\pi}{3} \frac{\alpha_i^2 \sigma_{i,w}^3}{\left[R_v T \ln\left(e_{s,w}/e_{s,i}\right)\right]^2}. \tag{9.6}$$

The dependence of $\Delta G^*_{i,w}$ on the saturation water vapor pressures with respect to bulk liquid water ($e_{s,w}$) and ice ($e_{s,i}$) can be understood by expressing $\ln(e_{s,w}/e_{s,i})$ as a function of the supercooling $T_0 - T$, according to eq. (3.91):

$$\ln \frac{e_{s,w}}{e_{s,i}} = \frac{L_f}{R_v} \frac{(T_0 - T)}{T_0 T} \tag{9.7}$$

and therefore

$$\begin{aligned} \Delta G_{i,w} &= -\frac{4\pi r^3 R_v T}{3\alpha_i} \frac{L_f}{R_v} \frac{(T_0 - T)}{T_0 T} + 4\pi r^2 \sigma_{i,w} \\ &= \underbrace{-\frac{4\pi r^3 L_f}{3\alpha_i} \frac{(T_0 - T)}{T_0}}_{\text{volume term}} + \underbrace{4\pi r^2 \sigma_{i,w}}_{\text{surface term}}. \end{aligned} \tag{9.8}$$

Besides the thermodynamic parameters, the kinetic parameters, such as the viscosity of the parent phase or the rate at which molecules can rearrange their orientation and join the ice lattice, determine the rate at which critical ice embryos form in the metastable parent phase. In extreme cases, the kinetics can slow or even inhibit ice nucleation even under thermodynamically favorable conditions (e.g., Berkemeier et al., 2014).

The Gibbs free energy barriers ΔG^* that need to be overcome for the three different homogeneous nucleation pathways to occur ($\Delta G^*_{w,v}$, $\Delta G^*_{i,v}$, and $\Delta G^*_{i,w}$) is evaluated as a function of T and S_w in Figure 9.4. The temperature dependencies of ΔG^* arise from the temperature dependencies of the saturation water vapor pressures ($e_{s,w}$, $e_{s,i}$), of the surface tensions ($\sigma_{w,v}$, $\sigma_{i,v}$), and of the interfacial tension ($\sigma_{i,w}$), given in Appendix A.3.

https://doi.org/10.1017/9781009485654.010 Published online by Cambridge University Press

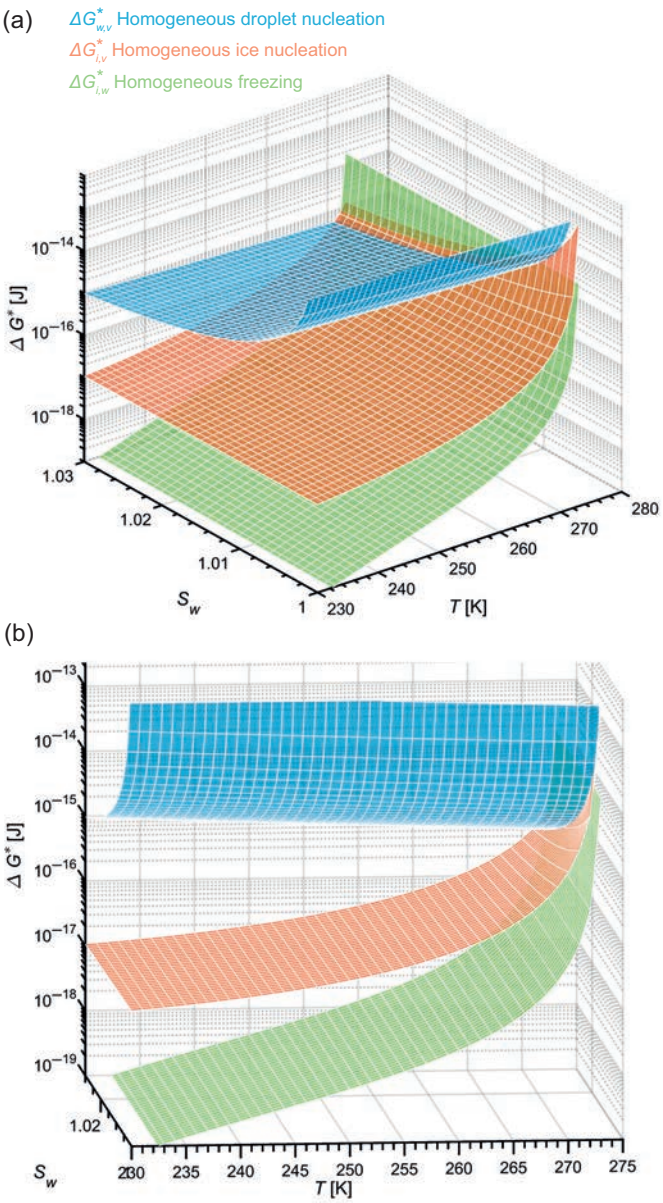


Figure 9.4 Energy barriers ΔG^* as functions of T and S_w that need to be overcome for (i) the homogeneous droplet nucleation $\Delta G^*_{w,v}$ (eq. 7.13), (ii) the homogeneous ice nucleation from the vapor phase $\Delta G^*_{i,v}$ (eq. 9.4), and (iii) the homogeneous freezing of a water droplet $\Delta G^*_{i,w}$ (eq. 9.6). Panels (a) and (b) show the same plot from different perspectives to better illustrate the trends.

$\Delta G^*_{w,v}$ depends only slightly on temperature but strongly on supersaturation (eq. 7.10). The weak temperature dependence of $\Delta G^*_{w,v}$ at a constant S_w is caused by the increase in $\sigma_{w,v}$ for decreasing temperature (Table 9.1), leading to a moderate increase in $\Delta G^*_{w,v}$ for decreasing temperature (Figure 9.4).

On the contrary, $\Delta G^*_{i,v}$ decreases with decreasing temperature at a constant S_w, despite an increase in $\sigma_{i,v}$ with decreasing temperature. The reason is that S_i increases more strongly with decreasing temperature at a constant S_w (as illustrated in Figure 3.12b for $S_w = 1$) than $\sigma_{i,v}$ increases, which dominates the energy barrier $\Delta G^*_{i,v}$ shown in Figure 9.4.

https://doi.org/10.1017/9781009485654.010 Published online by Cambridge University Press

Table 9.1 Water density ρ_l (Marcolli, 2017) and ice density ρ_i (Pruppacher and Klett, 1997) in kg m^{-3}, surface tensions in mN m^{-1} as functions of temperature: $\sigma_{w,v}$ for $T > 0\,°C$ (Vargaftik et al., 1983), $\sigma_{w,v}$ for $T < 0\,°C$ (Hrubý et al., 2014), $\sigma_{i,v} \approx \sigma_{i,a}$ from Hale and Plummer (1974), and $\sigma_{i,w}$ based on the fit given in Zobrist et al. (2007). The full equations describing the temperature dependencies are given in Appendix A.3.

T in °C	ρ_l	ρ_i	$\sigma_{w,v}$	$\sigma_{i,v}$	$\sigma_{i,w}$
−40		922.90		106.03	
−35	976.79	922.21	80.17	105.28	23.7
−30	982.51	921.50	79.57	104.53	24.6
−25	987.70	920.76	78.95	103.78	25.5
−20	992.21	920.00	78.32	103.03	26.4
−15	995.92	919.21	77.68	102.28	27.3
−10	998.74	918.40	77.01	101.53	28.2
−5	1000.64	917.56	76.34	100.78	29.1
0	1001.62	916.70	75.65	100.03	30.0
5	1001.75		74.95		
10	1001.12		74.23		
15	999.87		73.50		
20	998.16		72.75		
25	996.17		71.99		
30	994.07		71.20		
35	992.01		70.41		
40	990.10		69.60		

In contrast with homogeneous nucleation from the vapor phase, the interfacial tension $\sigma_{i,w}$ decreases with decreasing temperature (Ickes et al., 2015, and Table 9.1). Hence, $\Delta G^*_{i,w}$ strongly decreases with decreasing temperature and thus makes homogeneous freezing the most favorable process at all temperatures below 0 °C as compared with homogeneous nucleation from the vapor phase (Figure 9.4).

Comparing the critical radii for homogeneous ice nucleation from the vapor and the liquid phases further emphasize that freezing is the preferred process. The critical radius that needs to be overcome at −20 °C at water saturation for homogeneous ice nucleation from the vapor phase is ∼ 10 nm, according to eq. (9.1), but is only 2 nm for homogeneous freezing (see Figure 6.7 from Pruppacher and Klett, 1997). This finding is consistent with *Ostwald's rule of stages* (Ostwald, 1897), which is based on empirical observations. The rule states that a supersaturated parent phase (in our case, water vapor) does not directly nucleate into the thermodynamically most stable phase (in our case, ice) but rather into the thermodynamically next most stable or metastable phase (in our case, supercooled water). The next most stable phase is closest in free energy to the parent phase and thus minimizes the entropy production (Nývlt, 1995).

https://doi.org/10.1017/9781009485654.010 Published online by Cambridge University Press

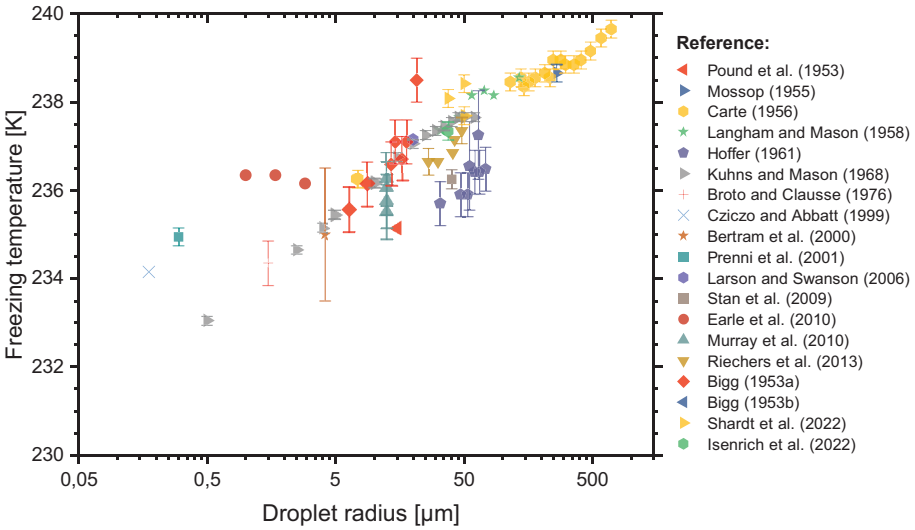


Figure 9.5 Examples of observed freezing temperatures of pure water droplets as a function of droplet size. Data are compiled from different experimental data sets, as indicated in the legend.

Based on experimental data on the freezing of pure water, it has been established that pure water droplets with a radius below approximately 5 µm freeze spontaneously only at temperatures below around 235 K as shown in Figure 9.5. At that temperature, the homogeneous freezing rate $J_{i,w}^{hom}$ becomes large enough that at least one nucleation event is likely to occur in a droplet of that size within an atmospherically relevant time period (Koop et al., 2000). Stochastically, homogeneous freezing is described as a Poisson process (Bigg, 1953*b*), where the freezing probability P of a droplet with volume V in a time interval Δt is given by

$$P = 1 - \exp(-J_{i,w}^{hom} V \Delta t). \tag{9.9}$$

Equation (9.9) shows that for constant $J_{i,w}^{hom}$ and Δt, P increases with increasing droplet volume, that is, with increasing radius. Therefore, the freezing temperature also increases with increasing droplet radius (e.g., Rau, 1953; Bigg, 1953*a*; Pruppacher, 1995) and as illustrated in Figure 9.5.

For example, a pure water droplet with a diameter of 1 mm already freezes homogeneously at temperatures around −25 °C (Bigg, 1953*a*). The temperature of −38 °C is known as the *homogeneous ice nucleation temperature* (HNT) of pure, micrometer-sized water droplets and delineates the colder cirrus cloud regime from the warmer mixed-phase cloud regime. In everyday life, one reason why we experience the freezing of water at temperatures very close to 0 °C is that often sufficiently large volumes of water are involved such that one nucleation event within seconds or minutes is likely to occur even at a low $J_{i,w}^{hom}$ value. Another reason is the presence of INPs (Section 9.1.2), with more INPs present in larger volumes of water.

The various ice nucleation pathways are shown in Figure 9.6 and described more in the following sections. Cloud droplets can be approximated as pure water droplets, which exist in equilibrium only at or above water saturation. Cloud droplets freeze homogeneously when supercooled to temperatures below 235 K, as indicated by Fr_{hom}^{CD} in Figure 9.6b.

https://doi.org/10.1017/9781009485654.010 Published online by Cambridge University Press

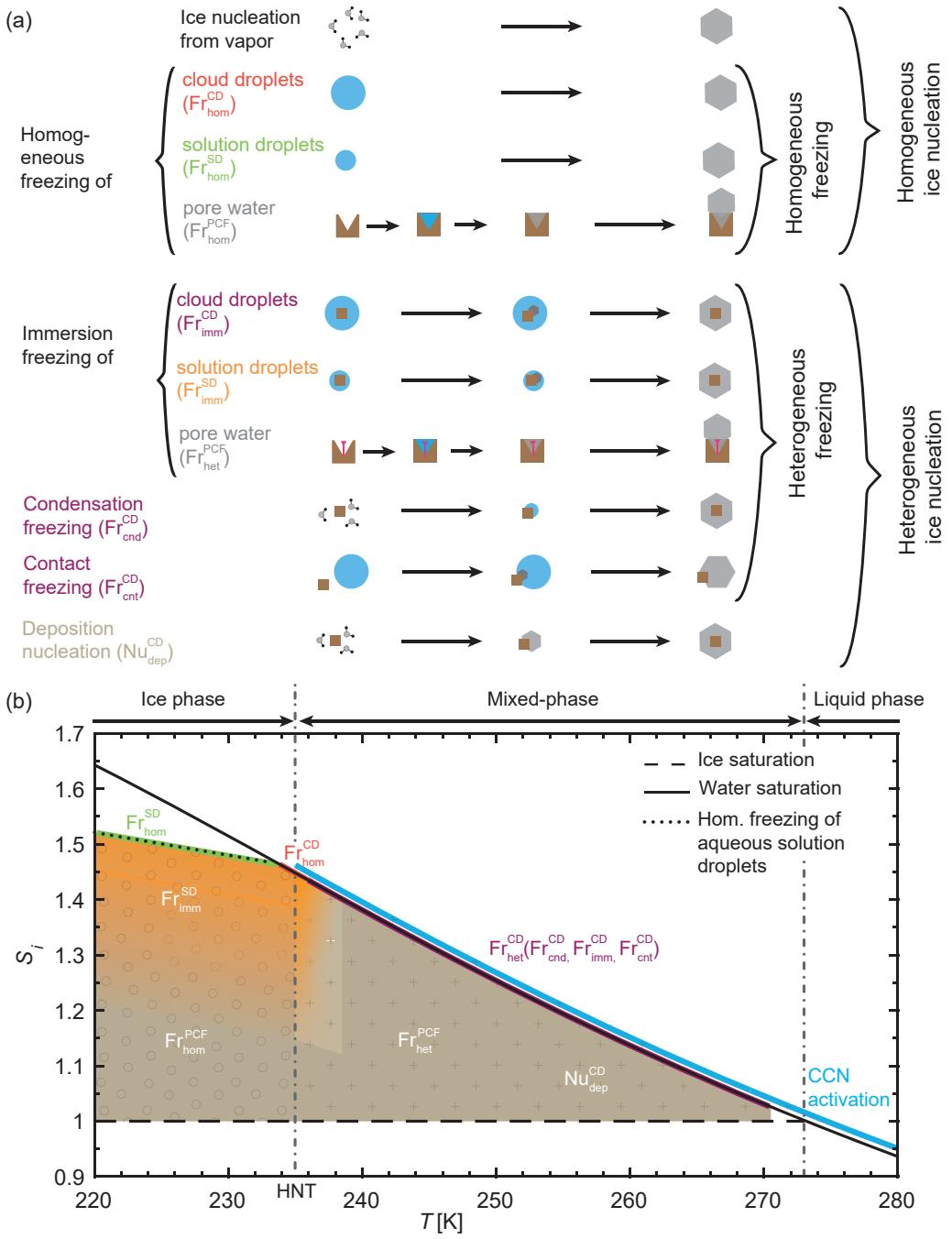


Figure 9.6 (a) Schematic of the individual ice nucleation pathways. The squares represent INPs, the circles droplets, and the hexagons ice crystals. (b) Schematic of the main atmospheric ice nucleation pathways as a function of T and S_i. The sloping dotted line starting at HNT (235 K) denotes the minimum saturation ratio for solution droplets to freeze homogeneously, according to Koop et al. (2000). The shaded areas denote the regions where the individual ice nucleation pathways depicted in panel (a) occur. The blue line denotes CCN activation, which precedes heterogeneous nucleation via immersion and contact freezing in the mixed-phase regime.

https://doi.org/10.1017/9781009485654.010 Published online by Cambridge University Press

Homogeneous freezing of supercooled cloud droplets occurs in deep convective clouds where temperatures below 235 K prevail. Homogeneous freezing also occurs in liquid-origin cirrus (Krämer et al., 2016; Wernli et al., 2016), nimbostratus, altostratus, or altocumulus, provided the temperature decreases below HNT.

Homogeneous Nucleation of Ice from Aqueous Solution Droplets

Adding solute to pure water changes the homogeneous ice nucleation conditions. Aqueous solution droplets require lower temperatures to freeze compared to pure water droplets. The difference in the homogeneous freezing temperature of pure, bulk water and that of a bulk aqueous solution is called *freezing* or *melting point depression*. This depression in melting point is illustrated in Figure 9.7 by the solid–liquid equilibrium line, which deviates increasingly more from the melting temperature of ice for decreasing water activities (i.e., increasing solute concentrations).

The homogeneous ice nucleation conditions for aqueous solution droplets can be related to the water activity (eq. 7.17) of the solution (Koop et al., 2000). Specifically, Koop et al. (2000) demonstrated that the HNT of aqueous solution droplets can be obtained by shifting the melting curve (i.e., the solid–liquid equilibrium shown as the dashed line in Figure 9.7) by a constant water activity offset Δa_w, as shown in Figure 9.7. The example droplet trajectory in Figure 9.7 illustrates that in the presence of a solute, the aqueous droplet first needs to take up water hygroscopically and grow into a suitable water activity range before it can freeze homogeneously. The constant offset in a_w has been shown to be valid for a range of different

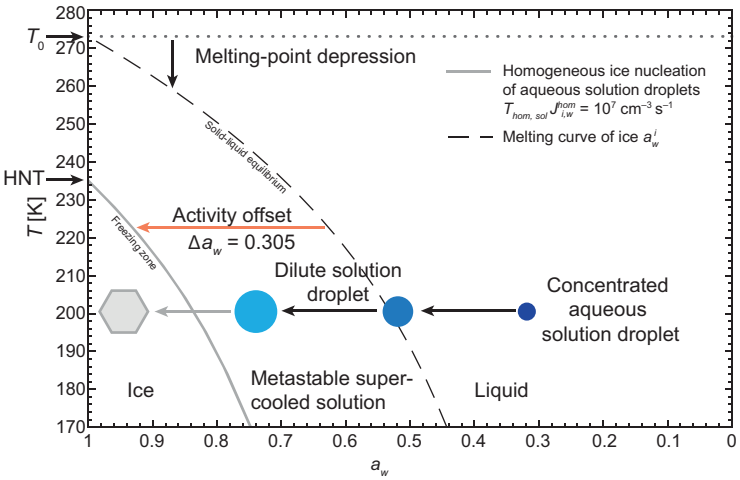


Figure 9.7 Melting curve of ice (a^i_w; black, dashed line), homogeneous freezing curve of aqueous solution droplets ($T_{hom,sol}$; gray, solid line) corresponding to a freezing temperature offset of $\Delta a_w = 0.305$ and a homogeneous nucleation rate $J^{hom}_{i,w}$ based on the parameterization given in Koop et al. (2000). Also indicated are the melting point temperature (T_0, dotted line) and the homogeneous nucleation temperature (HNT) of pure, micrometer-sized water droplets.

https://doi.org/10.1017/9781009485654.010 Published online by Cambridge University Press

solutes, including strongly dissociating acids such as sulfuric acid, salts such as ammonium sulfate, and dissociating organics (Koop et al., 1998; Bertram et al., 2000; Chen et al., 2000).

To reach the same homogeneous nucleation rate when the solution consists of 5 % salt ions ($a_w = 0.95$), the HNT needs to be lowered to 226.3 K, and to 216.5 K when 10 % of the solution consists of salt ions ($a_w = 0.90$). This is of importance for the homogeneous freezing of aqueous solution droplets in cirrus clouds formed in situ, where values of a_w down to 0.8 can be found at temperatures below 200 K (Koop et al., 2000). Cirrus formed in situ means that the ice crystals formed in the absence of a pre-existing cloud (Krämer et al., 2016; Wernli et al., 2016).

In fact, if the temperature is below −38 °C, RH is below water saturation, and no INPs are present, the homogeneous freezing of aqueous solution droplets is the only process that can lead to ice formation. In this case, where no liquid cloud droplets exist, aqueous solution droplets offer a liquid phase that can freeze homogeneously given that the supersaturation is high enough. The minimum saturation ratio required for the homogeneous freezing of aqueous solution droplets is shown by the dotted line in Figure 9.6b (Fr_{hom}^{SD}), corresponding to the solid gray line ($T_{hom,sol}$) in Figure 9.7.

It is still a matter of debate whether in situ formed cirrus clouds are mainly formed homogeneously (Spichtinger and Krämer, 2012) or whether sufficient INPs exist to cause widespread heterogeneous nucleation (Cziczo et al., 2013; Froyd et al., 2022). The former implies that the relative humidity in in situ formed cirrus clouds exceeds the threshold for the homogeneous freezing of aqueous solution droplets (Fr_{hom}^{SD} in Figure 9.6b) but generally does not reach water saturation (Jensen et al., 2005; Lawson et al., 2008; Krämer et al., 2009), consistent with cirrus forming during fast updrafts (Krämer et al., 2020). The latter implies that on average, lower ice supersaturations exist in the atmosphere, consistent with cirrus forming during slow updrafts (Krämer et al., 2020). The results for cirrus formed at different updraft speeds are qualitatively the same as those shown for properties in warm clouds as a function of updraft speeds in Figure 8.6.

9.1.2 Heterogeneous Ice Nucleation

Ice formation with the involvement of INPs is termed *heterogeneous ice nucleation*. INPs are particles that provide a foreign surface onto which water molecules are likely to adsorb, bond together, and form clusters with an ice-like structure, which can grow, ultimetly leading to the formation of a macroscopic ice phase (Vali et al., 2015; Kanji et al., 2017). In contrast to CCN, only a very small fraction of all aerosol particles can serve as INPs (Rogers et al., 1998; DeMott et al., 2010). This fraction can be as low as 10^{-7} in the free troposphere (Gao et al., 2024) and as high as 1 at the HNT. The reason for their low abundance is that heterogeneous ice nucleation strongly depends on distinct surface features of the INPs. For CCN, on the contrary, surface features do not matter because they become aqueous solution droplets when the DRH is reached (Section 7.3). Therefore, the prerequisites for aerosol particles to act as INPs are less well understood than their ability to act as CCN.

An INP promotes the ice nucleation process because it reduces the Gibbs free energy barrier for the formation of an ice germ by offering potential ice embryos a foreign surface to form

https://doi.org/10.1017/9781009485654.010 Published online by Cambridge University Press

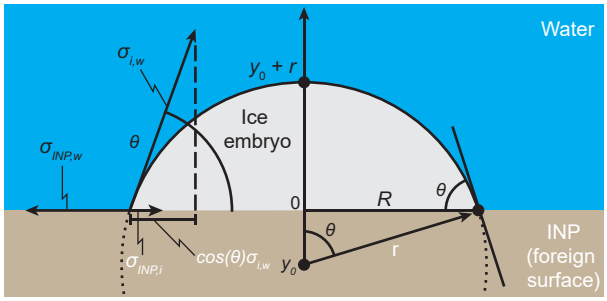


Figure 9.8 Schematic of the contact angle θ of a cap-like ice embryo with radius r that is forming on a flat, foreign INP surface in liquid water. The center of the spherical meniscus is located at $y_0 = -r\cos\theta$, and $R = r\sin\theta$ is the radius of the circular cross section formed at the interface of the INP and the spherical cap. $\sigma_{i,w}$ is the surface tension between ice and liquid water, $\sigma_{INP,w}$ is that between the INP and liquid water, and $\sigma_{INP,i}$ is that between the INP and ice.

upon. This concept is often visualized with a *spherical-cap model* (Volmer, 1929; Pruppacher and Klett, 1997). According to this model, an ice embryo with the shape of a spherical cap forms on the surface of an INP (Figure 9.8). The interaction between the ice embryo, the INP surface, and the surrounding parent phase is incorporated in a contact angle, which denotes the angle between the INP and the spherical ice cap, and is a consequence of the surface tensions between the ice embryo, the substrate (the INP), and the parent phase. A schematic illustrating the influence of the contact angle is shown in Figure 9.8, for an ice embryo forming on a flat INP surface within a parent phase of supercooled liquid water. The same concept can be applied to an ice embryo forming within a supersaturated water vapor phase (air), when replacing $\sigma_{INP,w}$ by $\sigma_{INP,a}$, where the subscript "a" refers to air, and $\sigma_{i,w}$ by $\sigma_{i,a}$.

In the context of water droplets forming on surfaces, the contact angle θ is usually understood as a measure of the "wettability" of a surface. Small and large contact angles represent a hydrophilic and hydrophobic surface, respectively (Figure 9.9b). Similarly, for ice nucleation, a small θ value represents good "compatibility" of the ice embryo with the INP's surface and significantly reduces the Gibbs free energy barrier for nucleation, by strongly reducing the number of water molecules required for the ice embryo before it reaches its critical radius. A reduced number of molecules in turn reduces both the volume term and the surface term of the Gibbs free energy as compared with the case of homogeneous ice nucleation, from either the vapor or liquid phase (eqs. 9.1 and 9.5). However, because of the spherical cap geometry, this reduction is more important in the volume term. The relation between the surface tensions and θ is mathematically described by *Young's equation* (Young, 1805) and is illustrated in Figure 9.8. For heterogeneous nucleation, it is given by

$$\text{from a parent liquid phase: } \sigma_{i,w}\cos\theta = \sigma_{INP,w} - \sigma_{INP,i}, \tag{9.10}$$

$$\text{from a parent vapor phase: } \sigma_{i,a}\cos\theta = \sigma_{INP,a} - \sigma_{INP,i}. \tag{9.11}$$

https://doi.org/10.1017/9781009485654.010 Published online by Cambridge University Press

The INP lowers the energy barrier if the surface tension between the INP and the ice embryo $\sigma_{INP,i}$ is lower than that between the ice embryo and the parent phase ($\sigma_{i,w}$ or $\sigma_{i,a}$) plus that between the INP and the parent phase ($\sigma_{INP,w}$ or $\sigma_{INP,a}$).

The influence of the contact angle on ice nucleation is shown in Figure 9.9 in terms of the Gibbs free energy barrier for homogeneous and heterogeneous freezing using different contact angles at $T = 253\,\mathrm{K}$. It can be seen that ice nucleation is much more likely to occur for a good INP, one with a contact angle smaller than 45 °, compared to the homogeneous freezing case ($\theta = 180\,°$). Even a moderately good INP with a larger contact angle of 90 ° can reduce the Gibbs free energy barrier to about half the value required for homogeneous freezing. It is important to note that the critical radius remains the same for homogeneous and heterogeneous freezing, because it is the radius of the critical ice embryo. This reduction in the energy barrier in the case of heterogeneous freezing $\Delta G^*_{het,i,w}$ is taken into account by multiplying $\Delta G^*_{i,w}$ for homogeneous freezing by a compatibility parameter f_{het}:

$$\Delta G^*_{het,i,w} = f_{het}\,\Delta G^*_{i,w}. \tag{9.12}$$

Here, ΔG^* is given depending on the metastable parent phase by either the expression in eq. (9.4) or in eq. (9.6). For ice nucleation on a flat surface, f_{het} is often expressed as (Turnbull and Vonnegut, 1952):

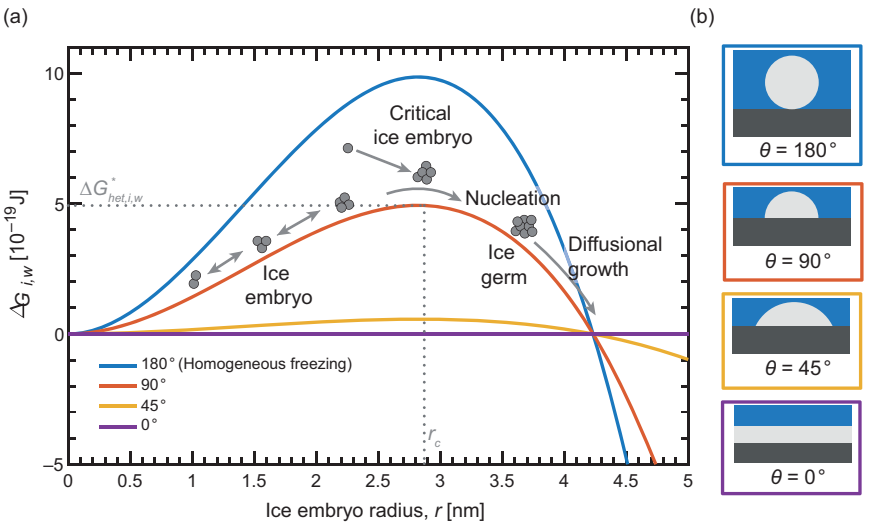


Figure 9.9 (a) Gibbs free energy barrier for homogeneous and heterogeneous freezing at $T = 253\,\mathrm{K}$ as a function of the embryo radius r, calculated using eq. (9.5). Heterogeneous freezing is presented for three contact angles, $\theta = 0\,°$, 45 °, and 90 °. The dotted horizontal and vertical lines indicate the Gibbs free energy barrier $\Delta G^*_{i,w}$ and the critical radius r_c for the case of the 90 ° contact angle. For the ΔG curves, ρ_i and $\sigma_{i,w}$ at 253 K were calculated according to Pruppacher and Klett (1997) and Zobrist et al. (2007), respectively (Appendix A.3). (b) Schematic illustration of the contact angles shown in (a); the dark gray areas show the INP and the blue areas the supercooled liquid water phase in which the ice embryo (shown in gray) forms.

https://doi.org/10.1017/9781009485654.010 Published online by Cambridge University Press

$$f_{het} = \frac{(2+m)(1-m)^2}{4}. \tag{9.13}$$

Here, m is the ice nucleation efficiency parameter, which is equal to $\cos\theta$. $f_{het} = 1$ for homogeneous freezing ($m = -1, \theta = 180\,°$), indicates that the particle surface does not promote ice nucleation and $f_{het} = 0$ for $m = 1, \theta = 0\,°$, corresponds to a perfect ice nucleus (Figure 9.9b).

In reality, the contact angle between ice and the INP surface is difficult to measure, especially because INPs can have complex surface structures (Section 9.1.5). Therefore, the ice-nucleating ability of different aerosol particles is usually analyzed in laboratory experiments. INPs can initiate freezing in several heterogeneous ice nucleation modes (Figure 9.6a), which will be discussed next.

Immersion Freezing

Immersion freezing refers to freezing that is initiated by an INP within a cloud or aqueous solution droplet. It requires that the INP has been already immersed in the cloud or aqueous solution droplet at higher temperatures. Upon cooling of the cloud or aqueous solution droplet, freezing is initiated (Figure 9.6a). Immersion freezing of aqueous solution droplets, such as oxalic acid (Zobrist et al., 2006; Wagner et al., 2011) or ammonium sulfate (Zuberi et al., 2001), can occur at temperatures below 235 K, where solution droplets exist (orange shading in Figure 9.6b).

In contrast to aqueous solution droplets, the immersion freezing of cloud droplets requires the prior existence of cloud droplets and thus relative humidities at or above water saturation (purple line in Figure 9.6b). Many studies have investigated the immersion freezing activity of cloud droplets initiated by different aerosol types (Murray et al., 2012; DeMott et al., 2015). The overall picture emerging from these studies is that biological aerosol particles dominate ice nucleation via immersion freezing at temperatures above approximately −10 °C and that mineral dust dominates immersion freezing at lower temperatures. Overall, immersion freezing of cloud droplets is regarded as the most effective primary ice formation mechanism in mixed-phase clouds (Murray et al., 2012).

Condensation Freezing

Condensation freezing occurs in a rising air parcel containing an INP that starts from water-subsaturated conditions (Figure 9.6a). When water saturation is reached, embryos of condensed water will form on the INP surface and can grow to sizes large enough to contain a critical ice nucleus and initiate freezing. As INPs in general contain at least a small amount of water-soluble material in addition to the insoluble part, they can act as CCN at water supersaturations of only a fraction of a percent. Therefore, condensation freezing can occur only in the narrow range of S_w values before the CCN is activated and immersion freezing in cloud droplets takes place (purple line in Figure 9.6b). Nonetheless, it remains a matter of debate if condensation freezing is truly distinct from immersion freezing on a microscopic scale (Vali et al., 2015).

https://doi.org/10.1017/9781009485654.010 Published online by Cambridge University Press

Contact Freezing

Contact freezing, also called collisional freezing (Figure 9.6a), refers to the freezing that occurs as a result of the collision of an INP with a supercooled cloud droplet (Ladino Moreno et al., 2013). It is thus limited by the collision rate between supercooled cloud droplets and INPs (Croft et al., 2010; Nagare et al., 2015). The collision rate in turn is determined by the collision efficiency E (eq. 6.19 and Section 8.2.1) between a droplet and an aerosol particle (Slinn, 1983; Ladino et al., 2011) and by the number densities and distribution of aerosol particles and supercooled cloud droplets available for collisions with each other. Since contact freezing requires the presence of a cloud droplet, it is shown on the water saturation line in Figure 9.6b. However, a particular kind of contact freezing can also take place for $\mathrm{RH}_w < 100\,\%$: an evaporating cloud droplet at water subsaturated conditions could shrink until the INP within the droplet comes in contact with its surface. This freezing pathway has been termed *contact nucleation inside out* (Durant and Shaw, 2005; Shaw et al., 2005).

Deposition Nucleation

Deposition nucleation refers to the formation of an ice phase by direct deposition of vapor onto an INP. Deposition nucleation requires that the environmental saturation ratio with respect to ice S_i is greater than unity, but is traditionally assumed to proceed without the formation of a liquid water phase (brown shading in Figure 9.6b). Deposition nucleation is found in cirrus clouds, when vapor is deposited onto, for example, mineral dust particles (Cziczo et al., 2013).

It is not clear whether deposition nucleation continues at $S_w > 1$ or whether it is then replaced by other heterogeneous nucleation mechanisms such as condensation or immersion freezing, as discussed by Welti et al. (2014) and Marcolli (2014). Overall, deposition nucleation does not seem to be important for the formation of mixed-phase clouds, as lidar observations have revealed that cloud droplets are present before ice crystals can form via heterogeneous freezing mechanisms in mixed-phase clouds (Ansmann et al., 2008; Westbrook and Illingworth, 2011).

9.1.3 Pore Condensation and Freezing

The traditional model of deposition nucleation involves a phase transition directly from the vapor phase to the solid phase, which is not favorable according to Ostwald's rule of stages (Ostwald, 1897). Instead, the formation of ice below bulk water saturation, which has traditionally been viewed as deposition nucleation, may in reality occur as *pore condensation and freezing* (PCF) (Christenson, 2013; Marcolli, 2014; David et al., 2019). During PCF, the condensate forms within the pores and cavities of an INP due to capillary condensation of water vapor at $\mathrm{RH}_w < 100\,\%$. This is possible because the capillary condensate is in equilibrium with the vapor phase at $S_w < 1$. Specifically, the concave curvature of the liquid surface in the pore causes the capillary condensate to have a lower equilibrium water vapor pressure compared to bulk water according to the Kelvin equation (eq. 7.15). This is sometimes referred to as an *inverse Kelvin effect* (Fisher et al., 1981; Marcolli, 2014) because the Kelvin effect described in

https://doi.org/10.1017/9781009485654.010 Published online by Cambridge University Press

eq. (7.15) discusses the formation of a convex surface. Once formed, the pore water can freeze by immersion/condensation freezing in case ice-active sites (Section 9.1.5) are available within the pore at $T > 235\,\mathrm{K}$, or it can freeze homogeneously if exposed to $T < 235\,\mathrm{K}$ (Marcolli, 2014). If PCF takes place at $T \leq$ HNT, it should be regarded as homogeneous freezing and not as a heterogeneous ice formation process, because the ice phase forms within the volume of the supercooled pore water by homogeneous freezing (Marcolli, 2020). Hence, despite that a porous particle is required for PCF, it was found to occur mostly at $T \leq$ HNT (Welti et al., 2014; David et al., 2019). This is termed Fr_{hom}^{PCF}, takes place in the dotted region in Figure 9.6b, and strongly depends on the pore properties (David et al., 2020). Conversely, if ice-active sites are present within the pore, they can trigger heterogeneous ice formation of the supercooled capillary condensate even at $T >$ HNT and $\mathrm{RH}_w < 100\,\%$. This is termed Fr_{het}^{PCF} and takes place in the region in Figure 9.6b with the + symbols.

9.1.4 Stochastic Versus Deterministic Ice Nucleation

One question, regardless of the mode of heterogeneous nucleation, is whether nucleation is a stochastic or a deterministic (singular) process. Two controversial hypotheses have been advanced.

The *stochastic hypothesis* assumes that although the surface of an INP reduces the energy barrier for nucleation as compared to the homogeneous case, the freezing process remains stochastic in nature and is described by a nucleation rate (eq. 9.3). In a sample of identical INPs (i.e., equal surface areas and contact angles), all will have the same probability per unit time that an ice embryo on their surface reaches its critical size by random fluctuations. For an individual INP, it is impossible to predict if and when a nucleation event occurs. According to the stochastic hypothesis, the fraction of frozen droplets in a population of supercooled cloud droplets increases with time at constant temperature and S_i. Furthermore, in a freezing experiment with a given set of supercooled droplets held at constant temperature or supersaturation, the sequence in which the droplets freeze is completely random (e.g., Alpert and Knopf, 2016).

The *singular hypothesis*, on the contrary, assumes that each INP has a distinct temperature or supersaturation at which it will trigger a nucleation event. Accordingly, heterogeneous ice nucleation is fully determined by the environmental conditions. If these are held constant, the fraction of frozen droplets in a population of supercooled droplets does not change with time. If a freezing experiment is repeated several times with the same set of droplets, the sequence in which the droplets freeze will always be the same.

According to CNT, heterogeneous nucleation is envisioned as a stochastic process. Experimental studies in which the time dependence of immersion freezing was investigated provide support for a stochastic component of the ice nucleation process (Murray et al., 2011; Niedermeier et al., 2011; Pinti et al., 2012; Welti et al., 2012) in addition to the deterministic nature. The deterministic component can be accounted for by assuming that not all INPs are the same but that some are more efficient and some are less efficient, that is, by accounting for so-called active sites, at which ice nucleation is preferentially initiated (Section 9.1.5). In conclusion, this means that heterogeneous nucleation has both a deterministic and a stochastic component (Vali, 2014).

https://doi.org/10.1017/9781009485654.010 Published online by Cambridge University Press

9.1.5 Ice-nucleating Particles (INPs)

Types of Ice-nucleating Particles

Heterogeneous ice nucleation proceeds on different types of atmospheric aerosols (e.g., Murray et al., 2012; Hoose and Möhler, 2012; Kanji et al., 2017). A compilation of the "onset" temperatures and S_i at which ice nucleation was first observed for different aerosol particle types in previous laboratory studies is shown in Figure 9.10, based on data from Hoose and Möhler (2012). Onset temperatures and saturation ratios generally refer to the highest temperature and lowest saturation ratio at which ice was detected in an experiment. The shown onset conditions are affected by the detection limit of the various instruments, especially their size thresholds. Nevertheless, the data allow us to identify typical temperature and supersaturation regions where the different aerosol types and ice nucleation pathways are active. Figure 9.10 includes deposition nucleation, condensation freezing, and immersion freezing for bioaerosols (bacteria, fungal spores, and pollen), mineral dust particles, OA, ammonium sulfate particles, and soot particles. Condensation and immersion freezing refer to those symbols that lie at or above the bulk water saturation line. It can be seen that there is a considerable spread between the different data, caused by the variety of aerosol types within one category (e.g., montmorillonite, kaolinite, or Arizona test dust (ATD) in the mineral dust category) and the different experimental methods used. Note that the symbols that lie considerably above bulk water saturation are not atmospherically relevant.

The onset temperature and S_i values at which a certain INP initiates ice nucleation depend on the requirements for an INP and the heterogeneous ice nucleation mechanism

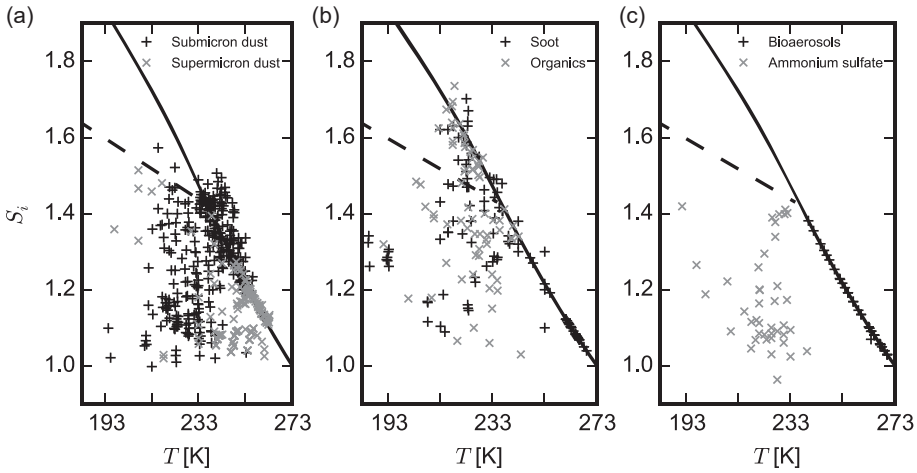


Figure 9.10 Onset temperatures (T) and environmental saturation ratios with respect to ice (S_i) for heterogeneous nucleation of (a) mineral dust, divided into sub- and supermicron aerosol particles, (b) organic particles and soot, and (c) bioaerosols and ammonium sulfate. The solid lines denote saturation with respect to bulk water ($S_w = 1$). The sloping broken lines refer to the onset conditions for the homogeneous freezing of aqueous solution droplets according to Koop et al. (2000). Onset conditions refer to a range of different ice activated fractions. Figure adapted from Hoose and Möhler (2012).

https://doi.org/10.1017/9781009485654.010 Published online by Cambridge University Press

(Section 9.1.2). While generally for most mineral dusts, bioaerosols, and crystalline ammonium sulfate particles (good INPs), heterogeneous ice nucleation occurs at considerably higher temperatures and lower supersaturations than those required for the homogeneous freezing of aqueous solution droplets, this is not the case for a large fraction of the soot types and OA (poor INPs). For the immersion and/or condensation freezing data shown in Figure 9.10 (symbols above the bulk water saturation line), the highest onset temperatures occur for bioaerosols, followed by mineral dust, and then OA. While bioaerosols are very efficient INPs (e.g., Morris et al., 2013), mineral dust is the most abundant atmospheric aerosol type by mass (Table 6.4), and it is well established that mineral dust is the most abundant INP in the atmosphere (DeMott et al., 2003; Froyd et al., 2022). Nonetheless, the ice nucleation ability of different dust types varies considerably (e.g., Zimmermann et al., 2008), with feldspar ranking among the most ice-active types (e.g., Atkinson et al., 2013; Harrison et al., 2019). By contrast, soot particles only become active as INPs below the HNT (Mahrt et al., 2018; Vergara-Temprado et al., 2018; Kanji et al., 2020), but even then quickly get outcompeted by mineral dust particles (Kärcher et al., 2023).

For the deposition nucleation and/or PCF data shown in Figure 9.10 (symbols below the bulk water saturation line), the highest onset temperatures and/or lowest S_i occur for mineral dust, followed by crystalline ammonium sulfate, OA, and soot.

The heterogeneous nucleation of mineral dust is further distinguished into sub- and supermicron mineral dust particles in Figure 9.10a. The lower onset S_i of the supermicron dust particles, independent of the ice nucleation pathway, reveals that the particle size is an important factor, as discussed next. Not included in Figure 9.10 are for example nano- and microplastic particles from anthropogenic emissions, which have also been reported to act as INPs (e.g., Aeschlimann et al., 2022; Seifried et al., 2024). In addition, sea spray aerosols, that constitute the aerosol types with the largest emission (Table 6.4), have also been reported to act as INPs (e.g., DeMott et al., 2016; Alpert and Knopf, 2016).

Requirements of INPs

The empirical criteria for an aerosol particle to act as an INP are (i) its size, (ii) providing a foreign surface (e.g., crystalline surface in the case of mineral dust or ammonium sulfate, or amorphous surface in the case of OA), (iii) its crystal lattice structure, (iv) its molecular bindings with water, and (v) its ice-active sites (Pruppacher and Klett, 1997).

(i) Atmospheric particles that can act as INPs generally have radii larger than 50 nm (Vali, 1966). Increasing ice nucleation efficiency with increasing particle size has been reported for mineral dust particles (e.g., Welti et al., 2009; Hoose and Möhler, 2012) and soot particles (e.g., Zhang et al., 2020; Gao, Friebel, Zhou and Kanji, 2022). The larger an INP, the larger the probability that a critical cluster forms on it within a given time span according to stochastic hypothesis (Section 9.1.4 Fletcher, 1958; Vali, 1966) and the larger the probability that its surface contains active sites. Therefore, data for all ice nucleation modes show higher ice nucleation temperatures and/or lower ice supersaturations for larger mineral dust particles (Figure 9.10a). According to CNT, the probability P for an ice nucleation event to occur in a given

https://doi.org/10.1017/9781009485654.010 Published online by Cambridge University Press

time span Δt and for a given heterogeneous nucleation rate J^{het} and surface area A of the INP's is given by:

$$P = 1 - \exp(-J^{het} A \Delta t). \tag{9.14}$$

Unlike for homogeneous ice nucleation (eq. 9.3), the heterogeneous ice nucleation rate is defined as the number of nucleation events per unit time and unit INP surface.

(ii) Atmospheric particles need to provide a foreign surface to significantly reduce the energy barrier for ice nucleation. This is because the foreign (often solid) surface enables an ice embryo on it to reach the critical radius with a lower number of water molecules in the ice phase than if the critical ice embryo were to form without a solid surface (Figure 9.8). Hence, crystalline mineral dust particles, the most common atmospheric INPs, are solid, insoluble substances. Aerosol particles that are solid only at certain temperatures and relative humidities can also act as INPs, such as crystalline salt particles (Abbatt et al., 2006; Wise et al., 2012), crystalline organics (e.g., Zobrist et al., 2006), and amorphous solid or glassy organics (e.g., Murray et al., 2010; Baustian et al., 2013).

(iii) A crystalline structure similar to an ice lattice is preferable for an INP (Weickmann, 1951), because water molecules can more easily arrange into an ice lattice on the substrate (Evans, 1965). Silver iodide (AgI) has lattice dimensions that are very similar to those of ice and nucleates ice at temperatures as high as −4 to −8 °C (Vonnegut, 1947; Marcolli et al., 2016), which is much higher than ice nucleation temperatures for mineral dust (Figure 9.11). Thus, AgI has been used as an INP in cloud seeding experiments to attempt to prevent hail damage (Federer et al., 1986; Dessens et al., 2016), increase precipitation in orographic clouds (French et al., 2018; Rauber et al., 2019; Benjamini et al., 2023), and understand glaciation of supercooled clouds (Henneberger et al., 2023). In the case of ice-nucleating bacteria, while the whole bacterium does not have a lattice structure, some of their proteins do show a structural resemblance to ice and promote ice nucleation (e.g., Wolber et al., 1986; Kajava and Lindow, 1993) when assembling into larger protein aggregates at interfaces (Roeters et al., 2021; Bieber and Borduas-Dedekind, 2024; Renzer et al., 2024). However, for certain aerosol particles that nucleate ice, the lattice match is completely missing (Head, 1961). Similarly, materials with a good crystallographic match with ice also have been reported to be poor INPs (Conrad et al., 2005). Thus, it is debatable how important this criterion is overall (e.g., Bi et al., 2017).

(iv) It has been suggested that for certain aerosol types, their ability to form hydrogen bonds with water matters for ice nucleation (Cox et al., 2015). For instance, montmorillonite has more available hydroxyl groups (-OH) than kaolinite and was reported to be more ice-active at −30 °C at the same S_i (Salam et al., 2006; Welti et al., 2009). In addition, montmorillonite is rich in sodium and calcium, which allow to take up water (Kumar et al., 2023). Nonetheless, results of molecular dynamics simulations suggest that there is still disagreement regarding the role of hydrophilicity for the ice nucleation activity of aerosol particles (Lupi and Molinero, 2014).

(v) Observations suggest that particles of the same size do not necessarily have the same ability to nucleate ice and that heterogeneous ice nucleation takes place on preferred sites on the INP surface, called ice-active sites (Fletcher, 1969). Ice-active sites can be imperfections such as crevasses, steps, or chemical functional groups on its surface or within pores of the

https://doi.org/10.1017/9781009485654.010 Published online by Cambridge University Press

INP (Fletcher, 1960; Zolles et al., 2015; Kiselev et al., 2017). Ice-active sites have been found to be distinct for different ice nucleation pathways (Holden et al., 2021). In the framework of CNT, these active sites can be interpreted as spots with a locally significantly reduced contact angle compared with the surrounding INP surface.

In summary, the ice-nucleating ability of a particle is impacted by its size, phase state, lattice structure, molecular binding, low interfacial energy between the INP and ice, and the presence of ice-active sites. Nonetheless, these commonly cited empirical requirements for particles to act as INPs need to be viewed with caution, as they have not served as a full set of guidelines to identify INPs, as discussed previously for the example of the lattice match criteria. Thus, the question of what property, or which combination of properties, makes a particle ice-active, is still a matter of debate.

9.1.6 Measurements of Ice-nucleating Particles

The ability of aerosol particles to heterogeneously nucleate ice depends on particle properties as well as on environmental conditions such as temperature and relative humidity, and is often quantified in terms of an *activated fraction* or *frozen fraction*.

For example, in immersion freezing experiments, usually the frozen fraction f_f is defined as the ratio between the ice crystal number concentration N_i to the sum of N_i and the cloud droplet number concentration N_d:

$$f_f = \frac{N_i}{N_d + N_i}. \tag{9.15}$$

An example of immersion freezing results from laboratory experiments on size-selected aerosol particles of different types, namely ammonium sulfate ($(NH_4)_2SO_4$), ammonium nitrate (NH_4NO_3), mineral dust (kaolinite), and silver iodide (AgI), is shown in Figure 9.11. In these experiments, a single aerosol particle was immersed within an air-suspended droplet with a radius of $\sim 7\,\mu m$.

Figure 9.11a demonstrates that f_f increases with increasing supercooling. Comparing the f_f curves of the different aerosol types, it becomes obvious that AgI is the most efficient INP out of the particles types shown. For the data shown in Figure 9.11a, AgI initiates freezing already at 264 K, whereas kaolinite initiates freezing only at 243 K, consistent with results from other laboratory studies (e.g., Lüönd et al., 2010; Welti et al., 2012; Wex et al., 2014). These results suggest that 100 nm kaolinite particles are not efficient INPs in the immersion freezing mode. However, there is an increase in the freezing probability with increasing size of the kaolinite particles, as shown in Figure 9.11b. Comparing the temperature at which the f_f reaches a value of 0.5 reveals that it increases from $T_{50} = 237\,K$ for kaolinite particles of $r = 100\,nm$ to $T_{50} = 239\,K$ for kaolinite particles of $r = 400\,nm$. Similar trends have been observed in other studies (e.g., Lüönd et al., 2010; Welti et al., 2012; Hartmann et al., 2016). The freezing probability depends on the total surface area of the aerosol particles within a droplet, but does not depend on the droplet volume, if the droplet contains a single INP (Hartmann et al., 2016).

Ammonium sulfate and ammonium nitrate are included in Figure 9.11a as reference experiments for homogeneous freezing of aqueous solution droplets. As expected, both aerosol types do not show any significant freezing above 235 K and there is no considerable difference in

https://doi.org/10.1017/9781009485654.010 Published online by Cambridge University Press

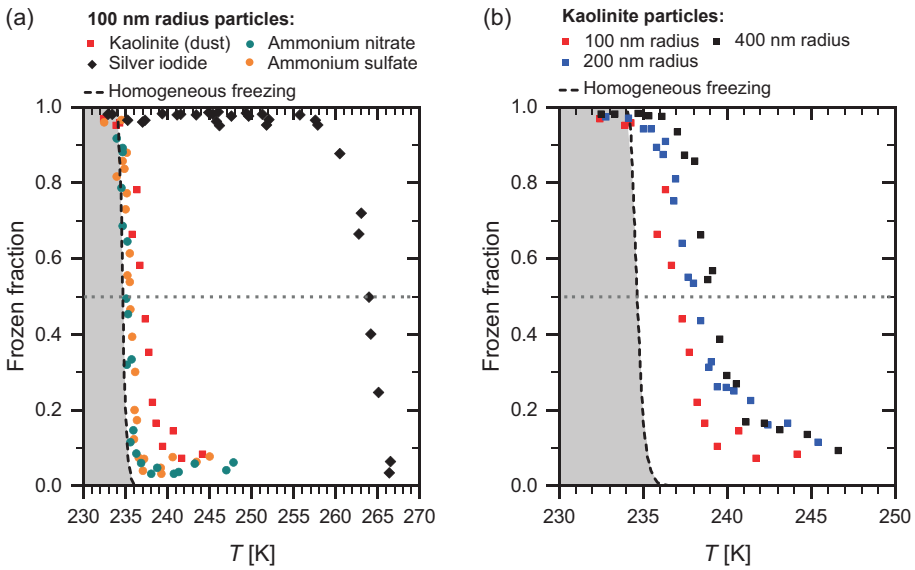


Figure 9.11 Frozen fraction (eq. 9.15) resulting from immersion freezing of droplets containing single immersed aerosol particles as a function of temperature for: (a) particles of 100 nm radius, including mineral dust (kaolinite), ammonium sulfate, and ammonium nitrate particles from Kohn et al. (2016), and silver iodide (AgI) particles from Lüönd et al. (2010), and (b) mineral dust (kaolinite) particles with different sizes from Kohn et al. (2016). In both panels, the shaded area indicates the temperature regime for the homogeneous freezing of aqueous solution droplets. Uncertainties are not shown for clarity, but are ± 0.4 K for temperature and approximately ± 3 % for the frozen fraction. The horizontal dotted lines indicate a frozen fraction of 50 %.

the freezing abilities of these two aerosol types nor to the freezing of pure water droplets of similar size.

Overall, the ice nucleation ability of aerosols, and hence the environmental INP number concentrations, depend strongly on temperature, as shown in the summary shown in Figure 9.12 (Kanji et al., 2017). However, there exists a variation in the INP concentration of three to five orders of magnitude at a given temperature. This spread is related to the requirements of INPs (Section 9.1.5). A striking aspect is the dominance of biological over marine particles at the highest subzero temperatures, with the former having about three orders of magnitude higher INP number concentrations. The overall picture emerging from previous studies of INPs is that INPs concentrations increase from 10^{-4}–1 L^{-1} at $T > -10\,°C$ to 10^{-1}–10^{4} L^{-1} between $-10\,°C < T < -40\,°C$ (Figure 9.12).

A rule of thumb for the dependence of INP number concentration on temperature was obtained by Fletcher (1962). Based on INP measurements available at that time, he found that there was about one INP per liter of air at $T = -20\,°C$, increasing by a factor 10 for each 4 °C of additional cooling at mixed-phase cloud temperatures. While an exponential dependence of the observed INP concentration on supercooling is accepted as typical (DeMott et al., 2016), it is recognized that the INP number concentration at any given location and time can be at least an order of magnitude smaller or larger than observed by Fletcher (1962).

https://doi.org/10.1017/9781009485654.010 Published online by Cambridge University Press

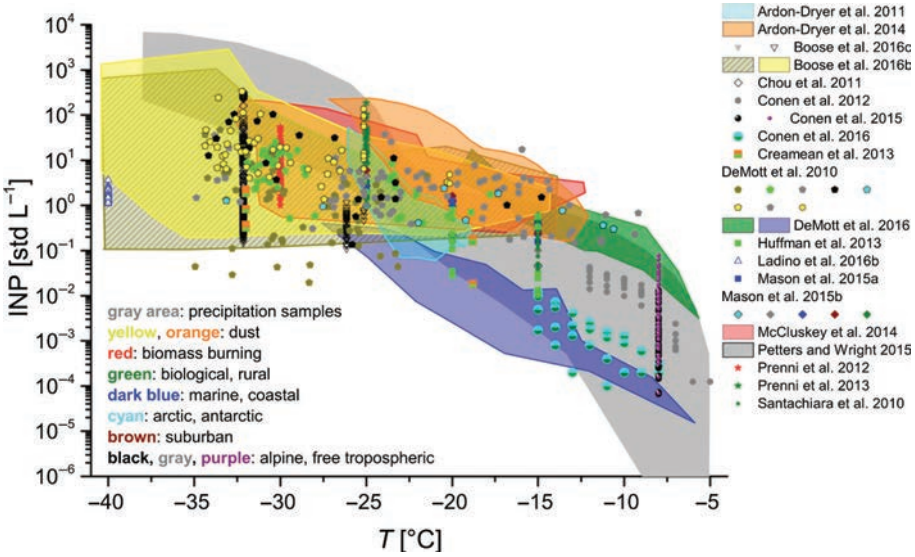


Figure 9.12 Compilation of INP number concentrations as a function of temperature for various field studies. Symbol colors indicate the airmass type and/or sampling location, corresponding to the colored fonts. INP concentrations are reported at standard conditions (1013 hPa). The shaded area and open symbols denote INP number concentrations for $RH_w < 100\,\%$ (deposition nucleation and/or PCF); all other areas and symbols denote INP number concentrations for $RH_w \geq 100\,\%$ (immersion and/or condensation freezing). Figure taken from Kanji et al. (2017). ©American Meteorological Society. Used with permission.

As shown in Figure 9.13, the primary ice crystal number concentration, being the one in the absence of ice multiplication or secondary ice processes (Section 9.4), is comparable to the number concentration of INP, but spans fewer orders of magnitude. It varies between 0.01 and 0.1 L^{-1} at a temperature of −8 °C and between 0.1 and 10L^{-1} at a temperature of −15 °C.

9.2 Ice Crystal Habits

Ice crystals exist in a manifold of different patterns and habits. The habit, that a growing crystal takes, is exclusively determined by the environmental conditions of temperature and supersaturation (Magono and Chung, 1966). Note that we refer to *habit* to indicate basic habits and to *shape* to indicate the entire crystal, which could have grown by collisions in addition to diffusion. A common basic habit of tropospheric ice crystals are hexagonal prisms in the form of plates and columns, both with 2 basal (hexagonal) faces and 6 prism (rectangular) faces, varying in their respective dimensions (Figure 9.14). Example photographs of different ice crystal habits are shown in Figure 9.15. Comprehensive classifications of the various ice crystals, snowflakes and graupel have been presented by several authors (e.g., Magono and Chung, 1966; Bailey and Hallett, 2009; Kikuchi et al., 2013).

https://doi.org/10.1017/9781009485654.010 Published online by Cambridge University Press

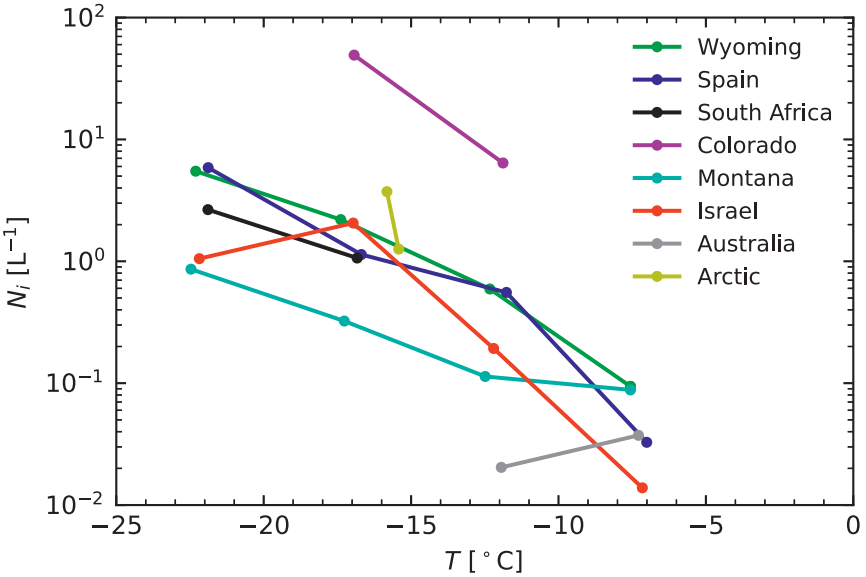


Figure 9.13 Observed ice crystal number concentrations N_i as a function of temperature at various locations in situations where secondary ice formation processes are assumed to be unimportant. Figure adapted from Vali (1985) with data added from Ny-Alesund in the Arctic (Pasquier et al., 2022).

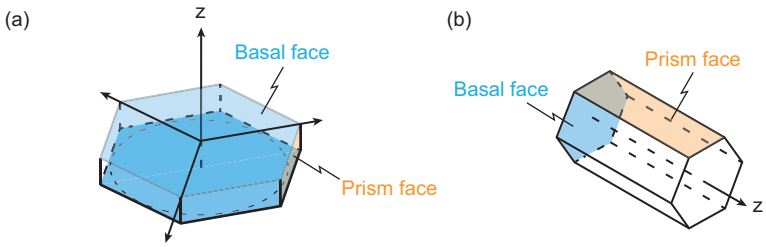


Figure 9.14 Schematic of the most common ice crystal habits: (a) plate and (b) column.

The equilibrium shape of a crystal, called *Wulff shape*, minimizes the amount of surface energy for a given volume (Wulff, 1901). Whereas CNT assumes that ice crystals are spherical, the reality is more complex owing to the ice lattice structure, where the surface tension at a crystal face depends on the orientation of that face with respect to the crystal lattice. For example, the surface tension of a basal face of an ice crystal and the surrounding water vapor phase, $\sigma_{i,v}^{B}$, was found to be lower than the surface tension of a prism face in water vapor, $\sigma_{i,v}^{P}$, by approximately 10% because the basal face has a lower density of hydrogen bonds (de Reuck, 1957; Pruppacher and Klett, 1997). In thermodynamic equilibrium, the ice crystal minimizes its surface-to-volume ratio, being a compact plate with a height to diameter ratio of 0.8 because of the lower surface energy of the basal face (Pruppacher and Klett, 1997). At high S_i, the ice crystals grow too rapidly to form the equilibrium shape and deviate the more from it, the higher S_i is (Lamb and Scott, 1972; Libbrecht, 2005). Here, ice crystal growth kinetics

https://doi.org/10.1017/9781009485654.010 Published online by Cambridge University Press

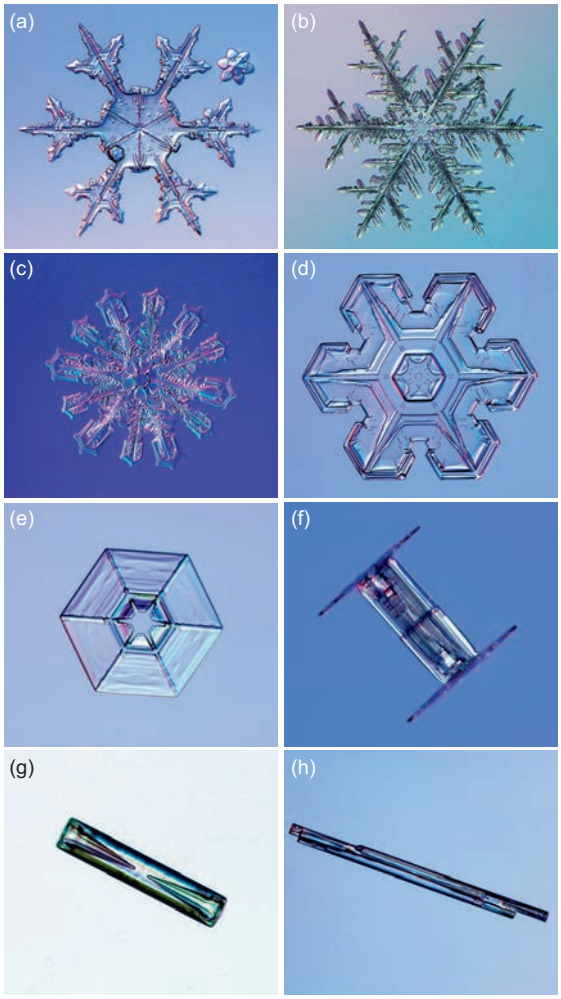


Figure 9.15 Photographs showing (a) a stellar dendrite, (b) a fern-like stellar dendrite, (c) a 12-sided ice crystal, (d) a stellar plate, (e) a plate, (f) a capped column, (g) a hollow column, and (h) a needle. Photographs taken from www.snowcrystals.com and used by permission and courtesy of Kenneth Libbrecht.

dominate over thermodynamics. If the growth of the hexagon preferentially takes place on the prism face, it results in a plate (Figures 9.14a and 9.15d,e). If growth on the basal face (growth along the z-axis) prevails, this leads to a column (Figures 9.14b and 9.15f,g). At high S_i, growth leads to dendrites (Figure 9.15a–c), needles (Figure 9.15h), stellar plates (Figure 9.15d), and hollow crystals (Figure 9.15g).

Some major ice crystal habits as a function of temperature and S_i are shown in Figure 9.16. This habit diagram is also known as *Nakaya diagram*, based on the initial categorization of laboratory generated ice crystals observed under different temperature and saturation conditions by Ukichiro Nakaya (Nakaya, 1954). At a given S_i, the growth is controlled by temperature. Between 0 and −5 °C and between −10 and −22 °C, the growth rate of the prism face exceeds that of the basal face, and vice versa between −5 and −10 °C (Lamb and Scott, 1972). These findings roughly agree with the observed morphology changes shown in Figure 9.16 from plates at temperatures higher than −3 °C, to columns between −3 and −10 °C, to plates between −10 and −40 °C and again predominantly to columns at temperatures between

https://doi.org/10.1017/9781009485654.010 Published online by Cambridge University Press

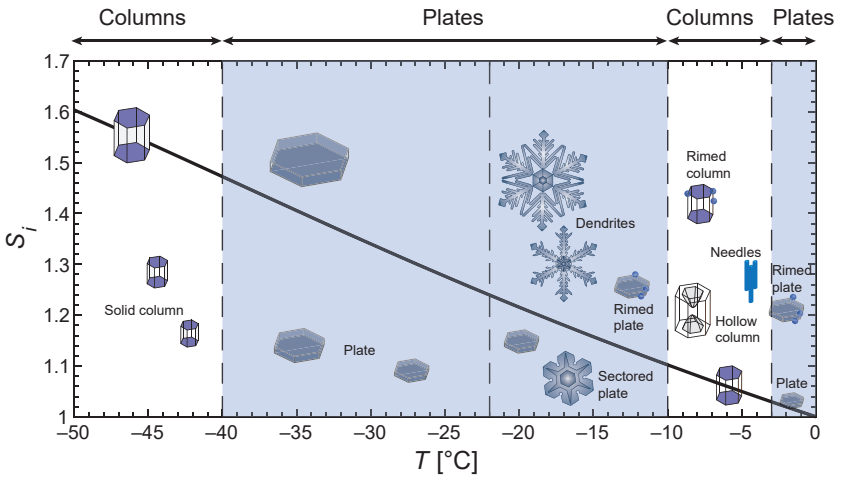


Figure 9.16 An ice crystal habit diagram, showing the various types of ice crystals that grow in air at atmospheric pressure, as a function of T and S_i. The solid line denotes saturation with respect to water.

−40 and −47 °C, depending on RH (Bailey and Hallett, 2009; Hueholt et al., 2022). At a given temperature, the ice crystal habits become more complex with increasing S_i. For instance, the columns forming between −3 and −10 °C are sturdy columns at the lower supersatruations and often more slender, hollow columns and clusters of needle-like crystals above water saturation (Libbrecht, 2005).

Larger snowflakes (aggregates made up of 10–100 or more individual crystals) often consist of dendrites and thin plates, indicative of diffusional growth conditions at high S_i. Far less common are aggregations consisting of columns and thick plates, which typically form well below water saturation.

At supersaturations above water saturation, rimed crystals of all shapes can be found (Figure 9.16). The percentage of supercooled liquid clouds increases with increasing temperature below 0 °C (Figure 1.19; Komurcu et al., 2014), and riming increases with increasing supercooled liquid water content, so riming also increases with increasing temperature. Riming is most pronounced in convective clouds with a high liquid water content and high vertical velocities (Table 1.3), as will be discussed further in Chapter 11.

Certainly within a given cloud, ice crystals may experience different temperature and supersaturation regimes. An ice crystal may start out growing in the column regime at temperatures between −3 and −10 °C and then be transported to either higher or lower temperatures, where plate growth dominates. In this regime, the ice crystal will develop plates at both ends of the column (e.g., Figure 9.15f), referred to as capped-columns (Kikuchi et al., 2013). If the ice crystal is then transported back to the column regime, columns will grow out of the plates, leading to ice particles that are termed columns on capped-columns (e.g., Pasquier et al., 2023).

Natural ice crystals are often less pristine than those shown in Figure 9.15. Examples of different ice crystals observed in the atmosphere are shown in Figure 9.17. Hence, while the

https://doi.org/10.1017/9781009485654.010 Published online by Cambridge University Press

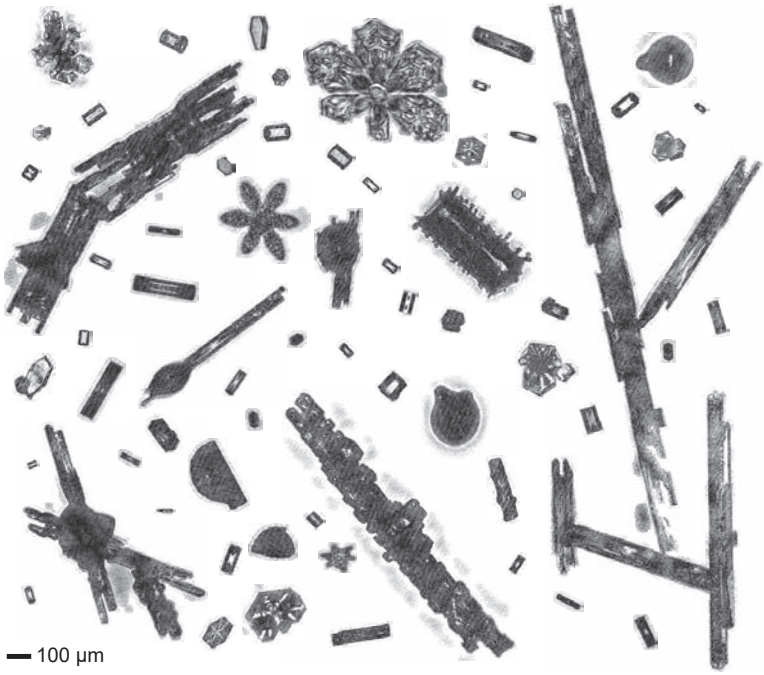


Figure 9.17 Photographs of different ice crystals observed in Ny-Alesund, Svalbard. The scale bar indicates the approximate size of the crystals. Figure provided by Jan Henneberger.

habit diagram in Figure 9.16 overall agrees well with in situ observations (Bailey and Hallett, 2004), it does not capture the entire variety of atmospheric ice crystals, which are often polycrystalline.

9.3 Ice Crystal Growth

Once an ice embryo has formed (Section 9.1), it will rapidly grow into a macroscopic ice crystal by vapor diffusion (Section 9.3.1). This is also called growth by deposition (Figure 9.1b). The environment will remain favorable for ice crystal growth as long as ice supersaturation is maintained. The growth processes for ice crystals as described later are analogous to those for cloud droplets, namely diffusional growth and growth involving collisions (aggregation and riming).

9.3.1 Growth by Diffusion

A newly nucleated ice crystal often grows more quickly by diffusion than a newly activated cloud droplet because it experiences higher supersaturations. For example, if the ice phase is nucleated within a supercooled cloud droplet, then RH is close to water saturation ($S_w \approx 1$), corresponding to, for example, an ice saturation ratio of $S_i = 1.22$ at $-20\,°C$ or of $S_i = 1.47$ at $-40\,°C$ (Figure 3.12). Hence, the newly nucleated ice crystal encounters a vapor phase at a significantly higher saturation ratio than that encountered by a newly activated cloud droplet, which typically only encounters S_w of 1.03 or less (Hudson et al., 2015). Therefore, for

https://doi.org/10.1017/9781009485654.010 Published online by Cambridge University Press

$T < 0\,°C$ at slight supersaturations with respect to liquid water, the water vapor gradient at the surface, driving diffusional growth, is larger for an ice crystal than for a cloud droplet.

In mixed-phase clouds, where ice crystals and supercooled cloud droplets co-exist, the ice crystals grow by diffusion at the expense of evaporating cloud droplets when the environmental water vapor pressure is between $e_{s,w}$ and $e_{s,i}$. This process is called the Wegener–Bergeron–Findeisen process (Figures 3.14 and 9.1c; Wegener, 1911; Bergeron, 1935; Findeisen, 1938), as discussed in Chapter 3. The Wegener–Bergeron–Findeisen process is more efficient if a mixed-phase cloud is mixed homogeneously in space than if the cloud consists of individual pockets of either ice crystals or supercooled cloud droplets (Korolev, 2007). In a homogeneously mixed mixed-phase cloud, the cloud droplets will evaporate more rapidly owing to their on-average closer proximity to the ice crystals. Eventually all cloud droplets will disappear and the saturation ratio will decrease to ice saturation. At this point, the Wegener–Bergeron–Findeisen process stops, if it has not yet been interrupted by the freezing of the remaining cloud droplets.

Ice crystals can grow by diffusion to tens of micrometers in only a few minutes. This occurs if their fall velocities are on the order of $0.1\,m\,s^{-1}$ so that they encounter new regions in the atmosphere where the vapor is not yet depleted (Fukuta and Takahashi, 1999). Individual ice crystals can even grow large enough to reach the ground as pristine crystals, highlighting the importance and efficiency of diffusional growth for ice crystals. For instance, in the Arctic, so-called *diamond dust* has been observed, which refers to ice crystal precipitation falling from a clear sky (Intrieri and Shupe, 2004). This *clear-sky precipitation* is attributed to very low INP number concentrations: the individual ice crystals grow quickly by vapor deposition because they do not need to compete for the available water vapor and at the same time are so sparse that no visible cloud is formed. They then sediment and reach the ground before colliding with other particles. Some drizzle or light rain also originates from unaggregated crystals which melted before reaching the ground.

The diffusional growth of an ice crystal (Figure 9.1b) requires the non-spherical shape of the ice crystal to be taken into account. Therefore, its growth is usually expressed in terms of mass rather than radius (Mason, 1953). Also, water vapor molecules cannot join the ice crystal in any random orientation, but must be oriented in such a way that the crystal structure is maintained. Thus, not every attempt of a water vapor molecule to join the crystal lattice is successful. These attachment kinetics are expressed by a mass accommodation coefficient α_m. Overall, the mass growth rate of a single ice crystal by vapor deposition, following initial formulations by Houghton (1950) and Mason (1953), can be expressed as:

$$\begin{aligned}\frac{dm_i}{dt} &= \alpha_m 4\pi C(S_i - 1)\left[\left(\frac{L_s}{R_v T} - 1\right)\frac{L_s}{KT} + \frac{R_v T}{e_{s,i}(T) D_v}\right]^{-1} \\ &= \alpha_m \frac{4\pi C(S_i - 1)}{F_k^i + F_d^i}.\end{aligned} \tag{9.16}$$

Here, m_i is the mass of the ice crystal, D_v is the mass diffusivity of water vapor in air (eq. 8.26), K is the thermal conductivity of air (eq. 8.24), and C is the capacitance, describing a shape parameter with units of length for nonspherical ice crystals. It has been shown that the

https://doi.org/10.1017/9781009485654.010 Published online by Cambridge University Press

diffusion equation describing the flux of water vapor to or from a cloud droplet or ice crystal is governed by equations analogous to those describing the electrical field around a conducting surface held at a given electrostatic potential (Houghton, 1950). This is why eq. (9.16) also contains a *capacitance* C. For a sphere, C equals its radius ($C = r$). Circular disks that are used as approximations for plate-type crystals have capacitance $C = 2r/\pi$. Empirically determined capacitances for other shapes can be found elsewhere (McDonald, 1963; Westbrook et al., 2008). Hence, knowledge of the relationship between m and C is needed to accurately predict ice crystal growth by deposition (Westbrook and Illingworth, 2011).

The mass growth rate given in eq. (9.16) results from integration of the flux of water vapor to the ice crystal over its surface. Eq. (9.16) is analogous to eq. (8.23) for cloud droplets if the constants F_k^i and F_d^i are defined with the respective terms for ice as follows:

$$F_k^i = \left(\frac{L_s}{R_v T} - 1\right)\frac{L_s}{KT} \qquad \text{and} \qquad F_d^i = \frac{R_v T}{D_v e_{s,i}(T)}. \tag{9.17}$$

In mixed-phase clouds, where the initial growth of ice crystals usually occurs at or close to water saturation (Korolev and Isaac, 2006), S_i can be approximated by $e_{s,w}/e_{s,i}$. As discussed in Chapter 8, growth rates generally depend on temperature and environmental pressure.

The mass accommodation coefficient α_m in eq. (9.16) was found to be ≤ 0.1 at temperatures between 233 and 273 K (Libbrecht and Rickerby, 2013; Kong et al., 2014), and it increases with decreasing temperature (e.g., Kong et al., 2014). Studies performed at $T < 233\,\text{K}$ have reported α_m values ranging over three orders of magnitude, as summarized by Choularton and Latham (e.g., 1977) and Haynes et al. (1992). On the whole, it has been suggested that attachment kinetics can be ignored in mass growth estimates when $\alpha_m > 0.1$, while for $\alpha_m < 0.1$ kinetic effects for crystal growth can generally not be ignored (Lamb et al., 2023). Nonetheless, the accommodation coefficient must be considered in order to capture changes in crystal habits. Furthermore, values of $\alpha_m < 1$ are required to explain ice crystal shape deviations from the equilibrium shape (Lamb and Scott, 1974; Nelson and Baker, 1996).

9.3.2 Terminal Velocity of Ice Crystals, Snowflakes, and Graupel

The determination of fallspeeds of ice particles is more complex than that of liquid hydrometeors due to the variety of shapes and densities of ice particles (Nakaya and Terada, 1935; Heymsfield, 1972; Locatelli and Hobbs, 1974; Heymsfield and Westbrook, 2010). Empirical functional relationships between the terminal fall velocity v_T ($\text{m}\,\text{s}^{-1}$), mass, and maximum dimension of the solid precipitation particles have been found. Typically, these relationships are power laws of the form

$$v_T = aD^b, \tag{9.18}$$

with coefficients a and b that describe the dependence of v_T on the hydrometeor diameter D. Here, D corresponds to the maximum dimension (D_{max}) of the solid particles (Locatelli and Hobbs, 1974; Mitchell, 1996), except for hail for which the equivalent spherical diameter

https://doi.org/10.1017/9781009485654.010 Published online by Cambridge University Press

Table 9.2 Empirical relationships for fall speeds of various frozen hydrometeor types. Fallspeeds are given in m s^{-1}, maximum dimensions D_{max}, and equivalent spherical diameters D_{eq}, in mm. Also indicated is the range of D (D_{max} or D_{eq}) values, over which the relationship has been suggested to be valid.

Hydrometeor type	Relationship between v_T and D	Valid range of D	Reference
Hail	$v_T = 11.45(0.1D_{eq})^{0.5}$	5 to 25	Mitchell (1996)
Conical graupel	$v_T = 1.2D_{max}^{0.65}$	0.8 to 3	Locatelli and Hobbs (1974)
Hexagonal graupel	$v_T = 1.1D_{max}^{0.57}$	0.8 to 3.2	Locatelli and Hobbs (1974)
Rimed column	$v_T = 1.1D_{max}^{0.56}$	0.8 to 2	Locatelli and Hobbs (1974)
Rimed dendrite	$v_T = 0.62D_{max}^{0.33}$	1.8 to 4	Locatelli and Hobbs (1974)
Plate	$v_T = 0.81D_{max}^{0.99}$	0.4 to 1.2	Locatelli and Hobbs (1974)
Dendrite	$v_T = 0.648(0.1D_{max})^{0.257}$	0.5 to 4	Mitchell (1996)

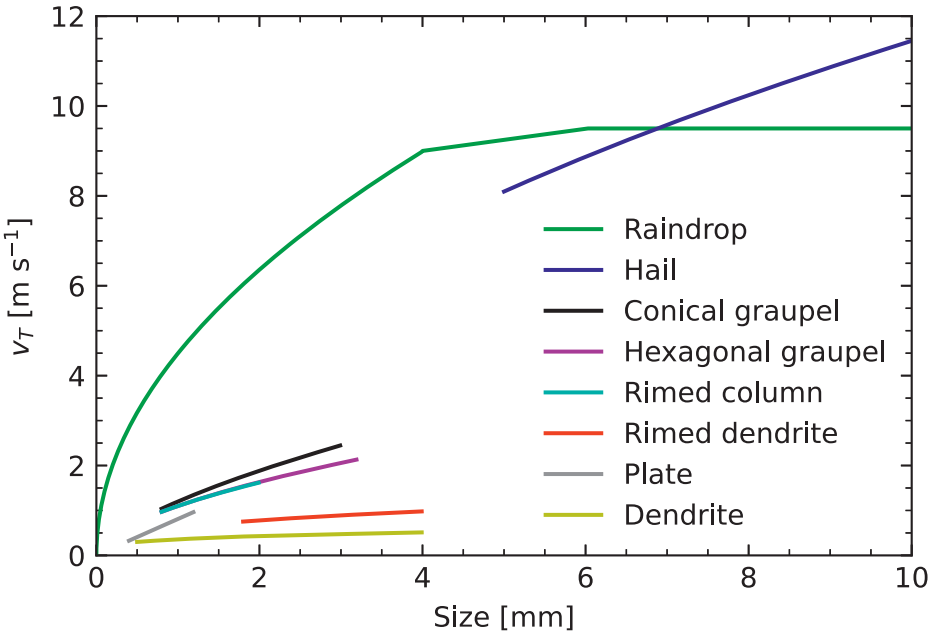


Figure 9.18 Terminal velocities of various hydrometeors as a function of their size (i.e., their maximum dimensions D_{max}, or, for hail, the equivalent diameters D_{eq}) for the parameterizations with their size limits as listed in Table 9.2 for solid hydrometeors from Locatelli and Hobbs (1974) and Mitchell (1996) and based on eq. 8.46 and Figure 8.12 for raindrops.

D_{eq} is usually used (Mitchell, 1996). Some examples are given in Table 9.2, and visualized in Figure 9.18.

Besides size, v_T also depends on the mass-to-area ratio of the falling hydrometeors. Therefore, it is desirable to have terminal velocity relationships, that in addition to the particle size, also depend on its mass and projected area (Heymsfield and Westbrook, 2010). For very flat (2D) snowflakes (dendrites) area and mass scale with r^2. Thus, the gravitational force F_G

https://doi.org/10.1017/9781009485654.010 Published online by Cambridge University Press

(eq. 8.36) is proportional to r^2, that is, it has the same radius dependence as the drag force F_D (eq. 8.37). Therefore, these quasi 2D dendrites can be observed to fall with nearly the same velocity for all sizes (Nakaya and Terada, 1935) (Figure 9.18). Analogously, raindrops with equivalent radii $\geq$2.5 mm become oblate spheroids and hence their terminal velocity levels off beyond equivalent radii of 3 mm. (Figures 8.12 and 9.18). While the terminal velocity of raindrops maximizes at 9–13 m s^{-1}, depending on the air density (Beard, 1976), the terminal fall velocity of snowflakes approaches at most only 2 m s^{-1}. The increase in fall velocity with increasing size is more pronounced for graupel than for rimed columns because $F_G \propto r^3$ for graupel (eq. 8.36). F_G's increase with increasing r is thus not compensated by the increase in drag force and therefore the graupel's terminal velocity continues to rise with increasing equivalent size. The terminal velocity of a graupel particle is smaller than that for a raindrop for the same size (Figure 9.18) because of the lower density of ice and because graupel particles also often have cavities filled with air. The terminal velocity of hailstones exceeds the one for raindrops of the same size, because hailstones remain conical or spherical and do not become oblate spheriods as raindrops do.

9.3.3 Growth of Ice Crystals Involving Collisions

Growth by Aggregation

An ice crystal can grow when colliding and clumping together with another ice crystal as indicated in Figure 9.1e. This process is called *aggregation* and leads to an aggregated snowflake (Figure 9.19e). Aggregation in cold clouds is thus the counterpart to growth by collision-coalescence of cloud droplets in warm clouds. However, the collection efficiency for aggregation is less well understood than that for the collision-coalescence process of cloud droplets (eq. 8.35). For ice crystals, the efficiency $\hat{E}$, with which the crystals remain together, is referred to as aggregation efficiency or *sticking efficiency*.

The sticking efficiency depends on temperature (Connolly et al., 2012; Phillips et al., 2015; Karrer et al., 2021), but studies disagree on the exact temperature dependence (Hobbs et al., 1974; Lin et al., 1983; Connolly et al., 2012). Overall, the temperature dependency of the sticking efficiency results from two main mechanisms, the sintering of crystals due to the presence of a *quasi-liquid layer* (QLL) (e.g., Slater and Michaelides, 2019) and the interlocking of dendrites.

The QLL generally describes a disordered layer with increased molecular mobility ("liquid-like"), which forms at temperatures below the melting point of any crystalline material (e.g., Nenow and Trayanov, 1986). This phenomenon is also referred to as pre-melting (e.g., Dash, 1989; Li and Somorjai, 2007). For ice, such a disordered interface has been reported at temperatures down to approximately 243 K (Bartels-Rausch et al., 2014). The presence of a QLL on ice was first postulated by Michael Faraday[1] in 1850, when investigating the ability of ice cubes to stick together (Faraday, 1860). The QLL of atmospheric ice crystals consists of a thin surface layer where the water molecules are neither in the rigid solid structure of the bulk ice nor in the random order of liquid water. This is because water molecules in the top layer of the

[1] www.britannica.com/biography/Michael-Faraday

https://doi.org/10.1017/9781009485654.010 Published online by Cambridge University Press

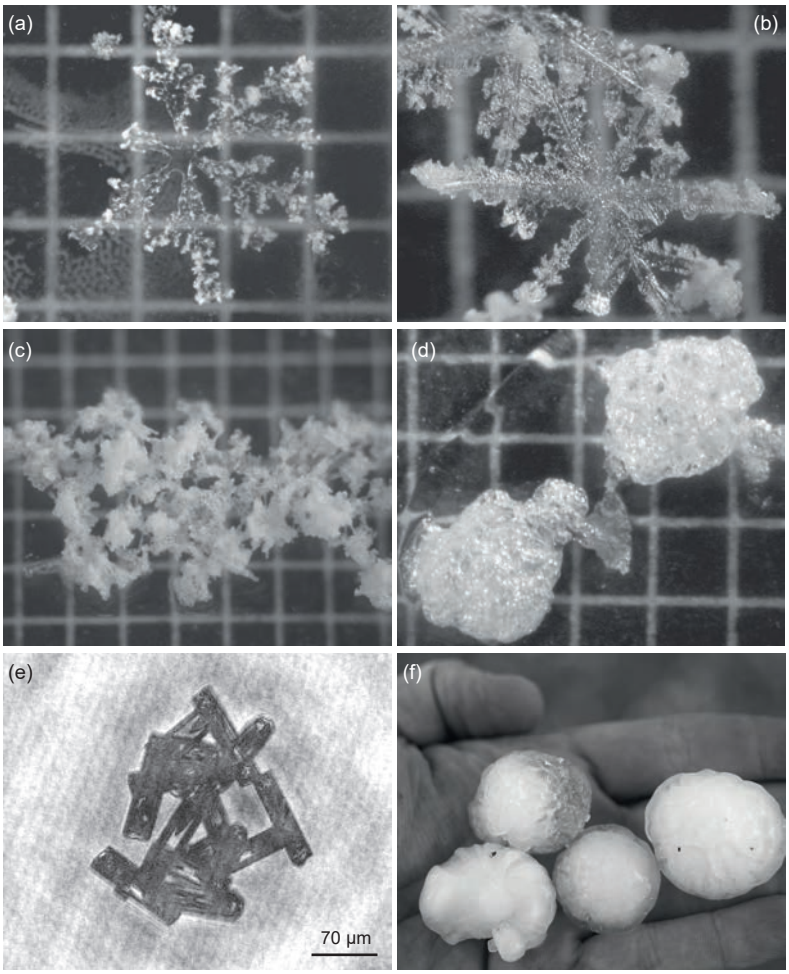


Figure 9.19 Images of different solid precipitation particles: (a) a lightly rimed dendrite, (b) two moderately rimed dendrites, (c) a densely rimed and aggregated ice crystal, (d) two graupel particles, (e) an aggregate, and (f) four hailstones. Photographs (a–d) are taken from Baschek (2005). Photograph (e) is by Christopher Fuchs and (f) is by Warren Faidley/The Image Bank/Getty Images.

ice have fewer neighboring molecules than in the crystal lattice. They are thus not completely trapped within a crystal structure but can move around to some extent, forming the QLL. The QLL is in equilibrium with water vapor on one side and with the bulk ice surface on the other side (Weyl, 1951). The QLL minimizes the surface energy of an ice crystal, because the surface tension between air and liquid water is smaller than that between air and solid ice ($\sigma_{w,a} < \sigma_{i,a}$).

The thickness of the QLL on ice surfaces increases with increasing temperature and has been reported to range from around 0.3 nm, that is, the diameter of a water molecule at 243 K, to a thickness of a few tens of nanometers at the melting point, though there is considerable spread

https://doi.org/10.1017/9781009485654.010 Published online by Cambridge University Press

in the reported temperature dependence of the QLL thickness (Bluhm et al., 2002; Bartels-Rausch et al., 2014). This thicker QLL at higher temperatures causes the sticking efficiency of ice crystals to be larger (Lin et al., 1983).

The process whereby two pieces of a solid substance stick together into a single solid body by the formation of intra-particle bonds is called *sintering*. Sintering of two colliding ice crystals is most effective within a few degrees of the melting point, owing to the presence of a thicker QLL (Szabo and Schneebeli, 2007). When two ice particles touch, the liquid at the contact point solidifies uniting the two particles (Blackford, 2007). This is in-line with the observation of Faraday, who suggested that a film of water on ice will freeze when placed between two pieces of ice, but retain in a liquid state whilst touching ice only on one side (Faraday, 1860). Sintering due to the QLL can explain observations showing that the aggregation process is mainly limited to temperatures higher than −10 °C, where it can result in large snowflakes (Hobbs et al., 1974; Houze, 2014). Sintering also explains why snow remains powdery at low temperatures but easily compacts to snowballs at higher (subzero) temperatures.

The maximum of the aggregation efficiency around −15 °C has been attributed to the presence of multi-branching dendritic ice crystals at these temperatures, which more easily interlock upon collision (Hobbs et al., 1974). This maximum corresponds to radar observations that revealed rapid aggregation at −15 °C with ice particles growing from 0.75 to 5 mm within less than 10 min (Barrett et al., 2019).

Other Types of Growth Involving Collisions

Various growth processes involving collisions are shown in Figure 9.1 and include (i) the collision–coalescence of differently sized drops with each other (Figure 9.1d and Section 8.2), (ii) the collision and aggregation of differently sized ice crystals (Figure 9.1e and Section 9.3.3), and (iii) the collision of an ice particle (ice crystal or snowflake) with a liquid particle (supercooled cloud droplet or raindrop) that freezes upon contact (Figure 9.1f), called *riming*. Photographs of different types of rimed ice crystals are shown in Figure 9.19a-c.

Growth involving collisions is caused either by the difference in fall velocities of the involved particles or by turbulence, both of which enable collisions between them. Whether the colliding particles remain together depends on the coalescence efficiency for liquid hydrometeors and on the sticking efficiency $\hat{E}$ when ice particles are involved. $\hat{E}$ of a cloud droplet or raindrop with an ice particle is approximately unity, because freezing is likely to occur upon contact with the supercooled cloud droplet or raindrop.

Riming leads to a hydrometeor whose density is between the density of a liquid hydrometeor and the density of a snowflake or ice crystal (Table 1.2), like graupel (Figure 9.19d, <2.5 mm in melted radius) or hailstones (Figure 9.19f if >2.5 mm in melted radius). These rimed particles are also classified as solid hydrometeors. Convective clouds with high vertical velocities are necessary for hailstones to form because the rimed particles need to be repeatedly caught in the updrafts, going through multiple cycles of riming (Section 11.4.1). A hailstone is denser than graupel because it can take up more liquid water prior to freezing. In graupel formation, the collected cloud droplets freeze more or less in their original shape, which leads to air cavities within graupel and therefore to a mass density well below that of bulk ice.

https://doi.org/10.1017/9781009485654.010 Published online by Cambridge University Press

The equation for growth involving collisions, in which the collector particle is an ice particle of equivalent radius R, is analogous to the growth leading to a raindrop (eq. 8.55):

$$\frac{dm_i}{dt} = \bar{\bar{E}} M_l \pi R^2 [v_T(R) - v_T(r)], \tag{9.19}$$

where M_l is either the liquid water content (in the case of graupel and hail) or the frozen water content (in the case of aggregates), $v_T(R)$ is the terminal velocity of the collector particle, $v_T(r)$ is the terminal velocity of the particle being collected, and $\bar{\bar{E}}$ is the mean collection efficiency over the full size range of collected particles.

9.4 Ice Multiplication (Secondary Ice Production)

Snowflakes can grow considerably larger than raindrops, as they tend to be rather two-dimensional and have a much lower density. This results in a lower fall speed of snowflakes compared to raindrops (Figure 9.18), which prolongs the time for interactions with other hydrometeors. While the coalescence efficiency of cloud droplets and raindrops depends mainly on their size, the sticking efficiency of ice crystals is mainly temperature dependent (Section 9.3.3) and decreases with decreasing sub-zero temperatures. Thus, upon collision with other hydrometeors at low temperatures, ice particles could, instead of sticking, break up into multiple ice particles. When this happens, it is called ice multiplication or secondary ice production (Field et al., 2017). Such events can help explain the ice crystal number concentration in mixed-phase clouds, which has frequently been observed to exceed the INP number concentration by more than an order of magnitude (e.g., Crosier et al., 2011; Lasher-Trapp et al., 2016; Mignani et al., 2019; Pasquier et al., 2022) as shown in Figure 9.20 (Wieder et al., 2022). While the first ice crystals form on INPs (primary ice), additional ice crystals may be produced by secondary processes in which the primary ice crystals are *multiplied*.

Secondary ice crystal production can occur by various processes: (i) the Hallett–Mossop or rime-splintering process, (ii) collisional break-up, (iii) droplet fragmentation upon freezing, (iv) thermal-shock fragmentation, (v) fragmentation of sublimating or melting ice, and (vi) activation of INPs in transient supersaturation of freezing droplets. The first three processes are the most common in the atmosphere and are described in more detail in the following.

(i) The Hallett–Mossop or rime-splintering process (Hallett and Mossop, 1974; Mossop and Hallett, 1974) refers to the production of secondary particles when supercooled drops of an appropriate size and temperature are captured by graupel, resulting in small secondary ice crystals (splinters) produced upon collision (Figure 9.1i). Secondary ice crystals produced by rime-splintering have been found to occur at temperatures between -3 and $-8\,^{\circ}\mathrm{C}$, with peak production occuring at $-5\,^{\circ}\mathrm{C}$, when cloud droplets larger than 12.5 μm in radius collide with graupel of at least 0.25 mm in radius (Mossop, 1985).

Another study observed that at $-5\,^{\circ}\mathrm{C}$ approximately 250 droplets greater than 12.5 μm in radius need to accrete on a graupel particle for one splinter to be released (Mossop, 1976). For a typical cloud droplet number concentration of $100\,\mathrm{cm}^{-3}$ (Figure 8.1 and Table 1.3), this

https://doi.org/10.1017/9781009485654.010 Published online by Cambridge University Press

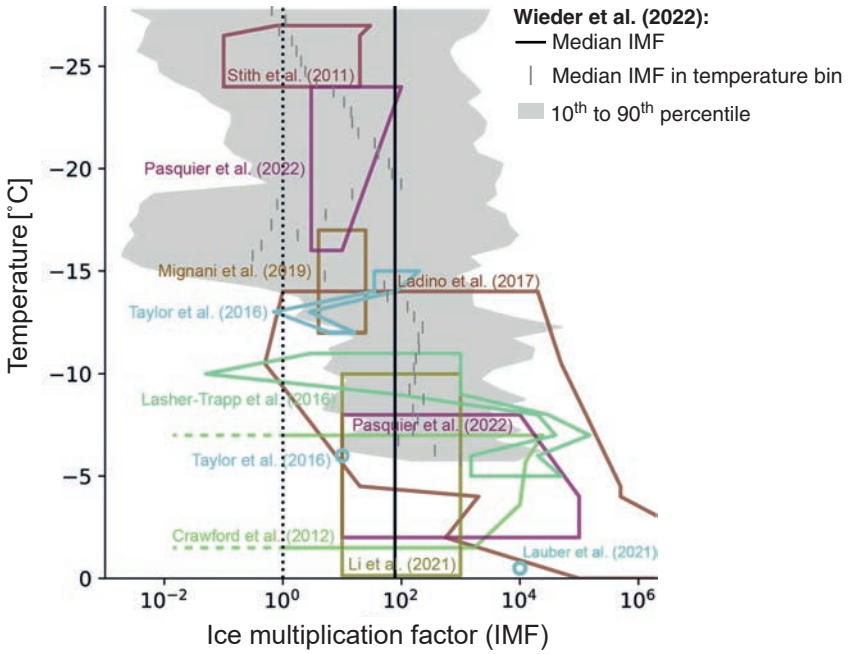


Figure 9.20 Summary of observed ice multiplication factors (IMF). Shown by the solid black line is the median IMF observed by Wieder et al. (2022) (gray shading indicating the 10th and 90th percentiles of observations with the median indicated by small vertical lines per temperature bin). The colored polygons represent IMFs observed in other field studies, as indicated. Figure adapted from Wieder et al. (2022).

yields an additional 0.4 ice crystals per cm^3, corresponding to an increase of up to four orders of magnitude at temperatures $> -8\,°C$. The suggested reason for the production of ice splinters during riming is the build-up of pressure within a freezing droplet, causing fragmentation (a little explosion, Choularton et al., 1978; Mossop, 1980). The narrow temperature range and the minimum size of the droplets for the Hallett–Mossop process are explained as follows: Between –3 to –8 °C, supercooled droplets accrete on the ice particle by a narrow ice bridge, keeping their identities. At temperatures higher than $-3\,°C$, droplets are thought to spread over the ice surface rather than remaining as discrete entities. At temperatures below $-8\,°C$, the freezing is thought to proceed so rapidly that the resulting ice shell is too thick to be disrupted (Mossop, 1985). More recent laboratory experiments, however, do not find any strong evidence for the Hallett–Mossop process (Emersic and Connolly, 2017).

(ii) Collisional break-up describes the break-up of an ice particle upon collision with another ice particle. It takes place when large ice particles (aggregates or graupel particles) have a sufficiently high collision kinetic energy (CKE) to cause break-up upon collision (Figure 9.1g) (Takahashi et al., 1995; Korolev and Leisner, 2020). This process was found to be most active at $-16\,°C$ (Takahashi et al., 1995), but was also reported to take place down to temperatures of $-24\,°C$ in Arctic clouds (Pasquier et al., 2022).

https://doi.org/10.1017/9781009485654.010 Published online by Cambridge University Press

(iii) Droplet fragmentation upon freezing of large droplets can also contribute to secondary ice production, as shown by laboratory studies (e.g., Lauber et al., 2018; Keinert et al., 2020). Due to the lower density of ice, pressure builds up inside the freezing drop, causing the ice shell to crack to release the pressure. Upon cracking, splinters can be ejected, which are a secondary source of ice crystals (Figure 9.1j). The number of splinters depends on temperature and was found to be highest at −15 °C (Keinert et al., 2020). Consistent with these laboratory studies, the presence of large droplets seems to preceed the increase in the ice crystal number concentration in observations of convective and orographic clouds (Lawson et al., 2017; Lauber et al., 2021).

As summarized in Figure 9.20, ice multiplication has been observed over a broad temperature range between 0 and −27 °C in various field studies. The ice enhancement factor is very variable ranging between no ice multiplication at all to ice crystal number concentrations that exceed the INPs concentration by up to six orders of magnitude (Wieder et al., 2022). Explaining the high ice enhancement factors remains a challenge, because of the diversity of conditions encountered in clouds.

9.5 Melting and Sublimation of Ice Particles

Snowflakes and ice crystals may not reach the gound because they can melt or sublimate on their way down. As the ice crystal structure at the surface starts to change into a QLL even at subzero temperatures, thermodynamically the new stable liquid phase is already present when the temperature approaches 0 °C. It is this interface with air at the edge of a piece of ice that explains the absence of a Gibbs free energy barrier and nucleation process for the melting of ice in all atmospherically relevant situations. By contrast, if melting is considered from a pure thermodynamic point of view, where no edges are taken into account, the liquid phase has to form within an infinite block of bulk ice, that is, an interface between the liquid and solid phase has to be formed in the presence of an energy barrier by nucleation. Hence, it is not surprising that melting always starts at the surface of crystalline substances (Dash et al., 1995). Because melting consumes energy, the temperature needs to exceed 0 °C for the melting of ice or snow to commence. The ice particles remain at 0 °C as long as the melting process is not complete even if the particle is in an environment with temperatures > 0 °C. Like the evaporation of raindrops, the sublimation of snowflakes depends on the relative humidity. Only if the RH is high enough for the snowflakes, graupel particles, or hailstones not to sublimate completely, will they reach the ground as precipitation.

9.6 Summary of Microphysical Processes in Warm and Cold Clouds

The microphysical processes discussed in this and the previous chapter are illustrated in Figure 9.1, depicting where the processes would occur in a convective cloud with a warm cloud base, a cold cloud top, and a mixed-phase zone in-between.

https://doi.org/10.1017/9781009485654.010 Published online by Cambridge University Press

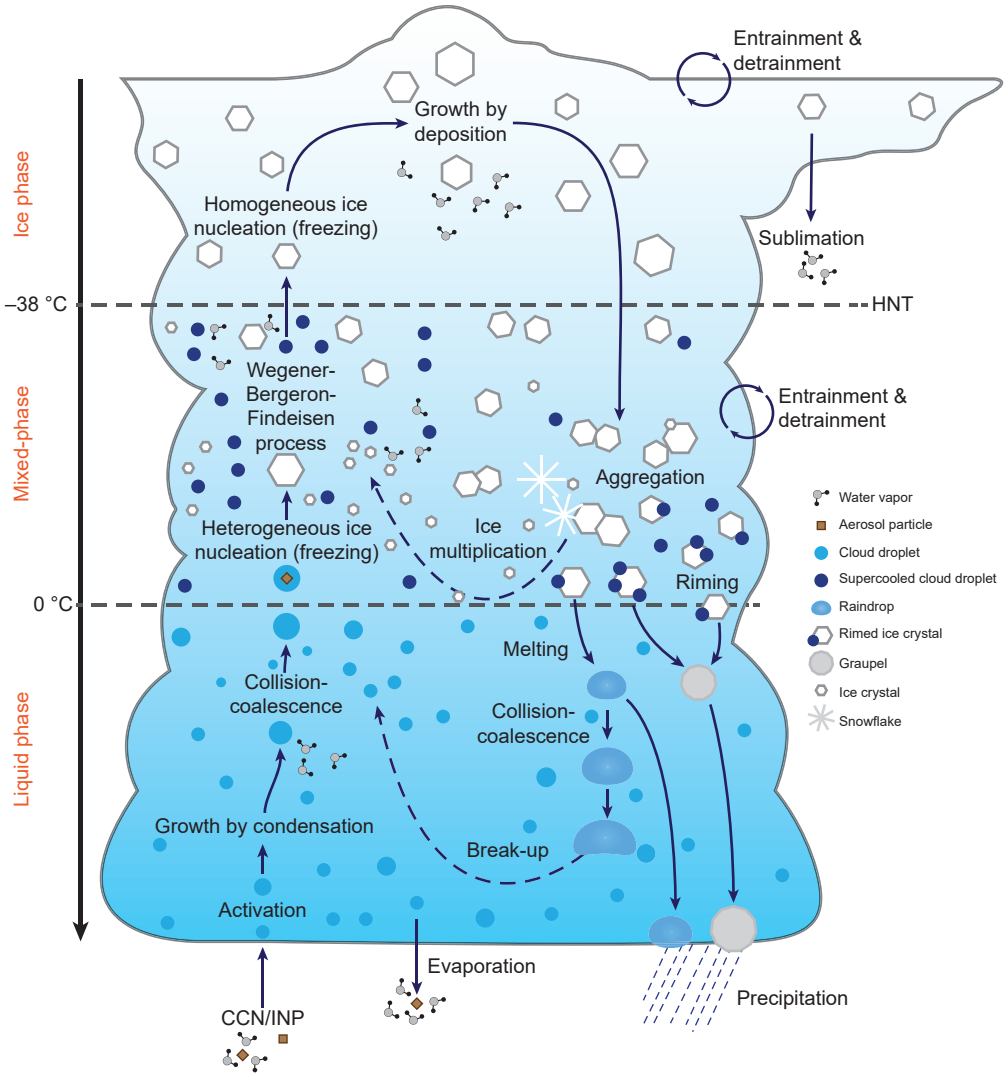


Figure 9.21 Microphysical processes occurring in a convective cloud with a cloud base temperature higher than 0 °C and a cloud top temperature lower than −38 °C, so that warm-, mixed- and ice-phase processes take place. The small arrows show typical trajectories of the temporal evolution of cloud particles.

In a cloud, droplets initially form through the activation of aerosol particles (Chapter 7). The droplets increase in size through condensational (diffusional) growth until some droplets are large enough for the collision–coalescence process to commence. If the cloud top extends to low enough temperatures, the first ice crystals will nucleate on INPs to form primary ice. Then, because of the difference in saturation water vapor pressure over liquid water and over ice, these ice crystals will grow by deposition at the expense of the evaporating cloud droplets (Wegener–Bergeron–Findeisen process, Figures 9.1c and 3.14) if the environmental water

https://doi.org/10.1017/9781009485654.010 Published online by Cambridge University Press

vapor pressure lies between saturation with respect to liquid water and ice. The Wegener–Bergeron–Findeisen process can cause this part of the cloud to become completely glaciated. Ice crystals grow further by deposition until they reach a large enough terminal velocity to fall against the updraft. Ice growth by deposition is the only growth mechanims at temperatures below −30 °C, where the QLL is extremely thin (Bartels-Rausch et al., 2014).

At higher subzero temperatures, the collection efficiencies involving ice crystals are higher because of their more substantial QLL, favoring growth by aggregation as the crystals fall to warmer regimes. Ice crystals and snowflakes will also grow by riming when they encounter supercooled cloud droplets. During riming and other collisions, secondary ice crystals can be produced that are small enough to be carried upward again in the cloud by the updraft, repeating the growth cycle. Ice crystals and snowflakes falling into regions of the cloud that are at temperatures above 0 °C will melt to drizzle or raindrops. If graupel and/or hailstones are present, it depends on the altitude of the 0 °C-isotherm, if they reach the ground as frozen particles or also melt into raindrops.

https://doi.org/10.1017/9781009485654.010 Published online by Cambridge University Press